Summer 2010

Simulation of PEM fuel cells: validation of model and incorporation of humidity dynamics

Steven Francis Rodgers

Department:

SIMULATION OF PEM FUEL CELLS: VALIDATION OF MODEL AND INCORPORATION OF HUMIDITY DYNAMICS

by

STEVEN FRANCIS RODGERS

A THESIS

Presented to the Faculty of the Graduate School of the

MISSOURI UNIVERSITY OF SCIENCE AND TECHNOLOGY

In Partial Fulfillment of the Requirements for the Degree

MASTER OF SCIENCE IN MECHANICAL ENGINEERING

2010

Approved by

Umit O. Koylu, Advisor
Scott E. Grasman, Advisor
John W. Sheffield

ABSTRACT

Fuel cell technologies have been receiving increased attention by industry and researchers due to growing societal and inevitable economic pressures to find an alternative for fossil fuels. At the forefront of this is the demand for fuel cell models: models to elucidate fundamental physical phenomena underlying fuel cell function and models that are not computationally demanding yet reasonably accurate to allow designers to incorporate fuel cells into consumer products. One of the latter type has recently been developed based on a software package that is already in widespread use in the automotive industry for the simulation of mechanical, thermal, electrical, and control systems of internal combustion engines and whole vehicle systems, and a functional proton exchange membrane (PEM) fuel cell model implemented in that package would help speed the design cycle of fuel cell and hybrid powered vehicles. The objective of this study was to analyze and test this model against independent experimental data available in the literature. Additional elements were then developed and integrated with the model to increase its predictive capabilities by enabling it to account for the effects of relative humidity and changes in temperature and pressure on the performance of fuel cells. This remedied observed deficiencies of the original model and allowed for more accurate simulations of variable fuel cell operating conditions.

ACKNOWLEDGMENTS

I would like to thank advisors, Umit Koylu and Scott Grasman, for their support and guidance on this project. This thesis would not have been possible without their input, and it is an honor for me to have worked with them. I would also like to thank my colleagues Shravan Vudumu and Isaiah Kellogg for their knowledgeable advice and friendship.

I am grateful for the United States Department of Energy for funding this project, and for the millions of taxpayers who unknowingly gave a portion of their income to support my small contribution to the body of technical literature.

I would like to thank the Missouri University of Science and Technology and the Department of Mechanical and Aerospace Engineering, which has been my home for the last quarter of my life. The staff and instructors here have helped me to become knowledgeable about topics I hardly knew existed when I first came here, but now delight in. I have unbounded appreciation for my early educators as well, specifically Tim Strzechowski and Joyce Zywica, who nurtured the skills of critical thinking and thoughtful analysis in the context of literary criticism, and Mary Cunningham, who showed me the joy of science and the infinite usefulness of unit analysis, which was invoked many times during the course of this project.

I am eternally indebted to my father, who showed me what it means to be curious about the universe, and my mother, who has tried to teach me not to procrastinate. Perhaps one day I'll learn.

TABLE OF CONTENTS

Page

LIST OF ILLUSTRATIONS

Figure Page

LIST OF TABLES

NOMENCLATURE

Symbol	Description	Units
A	Fuel cell active surface area	cm^2
a_{avg}	Average water activity across the fuel cell	
C_P	Product concentration density	mol/cm^2
C_R	Reactant concentration density	mol/cm^2
$\overline{C_R^o}$	Concentration of reactant in the bulk flow stream	mol/m^3
d	Membrane thickness	cm
D^{eff}	Effective diffusivity of oxygen in the gas diffusion layer	cm^2/s
F	Faraday constant	C/mol
ΔG	Activation energy	J
$\Delta \hat{g}_f$	Gibbs free energy	J
I	Fuel cell current	A
i	Current density	mA/cm^2
i_l	Limiting current density of the fuel cell	A/cm^2
i_o	Exchange current density	mA/cm^2
$\dot{n}_{gas}$	Molar flow rate of non-vapor gases in the cathode side	mol/s
$\dot{n}_{gas,in}$	Molar flow rate of non-vapor gases in the inlet stream	mol/s
$\dot{n}_{H_2O,in}$	Molar flow rate of water vapor in the inlet stream	mol/s
$\dot{n}_{H_2O,prod}$	Molar production rate of water vapor from the fuel cell	mol/s
$\dot{n}_{O_2}$	Molar flow rate of oxygen in the cathode side	mol/s
P_{anode}	Pressure of anode chamber	Pa
P_{avg}	Average pressure of cathode and anode chambers	Pa
P_{cath}	Pressure of cathode chamber	Pa
P_{H_2O}	Partial pressure of water in the fuel cell	Pa
$P_{H_2O_i}$	Partial pressure of water in the inlet stream	Pa
$P^*_{H_2O_i}$	Saturation pressure of water in the inlet stream conditions	Pa
R	Gas constant	J/(K*mol)
R_i	Membrane ionic resistance	Ω

T	Average fuel cell temperature	K
T_i	Temperature in the inlet stream	K
$\dot{V}$	Total (sum) volumetric flow rate of the fuel and oxidizer streams	m^3/s
X_{H_2}	Mole fraction of hydrogen in the anode chamber	
$X_{H_2 i}$	Mole fraction of hydrogen in a dry stream	
X_{O_2}	Mole fraction of oxygen in the cathode chamber	
$X_{O_2 i}$	Mole fraction of oxygen in a dry stream	
α	Charge transport coefficient	
δ	Thickness of the gas diffusion layer	cm
η_{act}	Activation overpotential	V
η_{mt}	Mass transport overpotential	V
η_{ohm}	Ohmic overpotential	V
λ	Ratio of H_2O to $SO_3^- H^+$ sites in the membrane	
σ	Membrane proton conductivity	S/cm
σ_{303}	Membrane proton conductivity at 303K	S/cm
ϕ	Average relative humidity of the cathode and anode inlet streams	
$\Delta\phi$	Interface potential	V
Ω	Membrane resistance	Ω
ΔE	Activation energy	J/mol

1. INTRODUCTION

Earth's supply of hydrocarbon fuels is finite and the rate at which geological processes create hydrocarbons has been greatly outpaced by their consumption by our modern society. It is clear then that an alternative, or many alternatives, to hydrocarbon fuels must be identified. An increased understanding of the impact human activities can have on the biosphere demands that the successors to our current power paradigm be environmentally friendly, and the reality of anthropogenic climate change necessitate finding a solution sooner rather than later.

Hydrogen provides a unique opportunity to reliably generate power with zero on-site emission of pollutants or greenhouse gases. While power from wind and solar sources are not always available, energy from hydrogen is accessible on demand. Hydrogen is an energy storage medium—since it does not exist in its elemental state on earth, it must be manufactured (potentially with renewable sources (Goswami et al., 2003)), and that takes energy. In this sense, it is more akin to a battery than a solar panel. As such, it can mediate between the arbitrary nature of some renewable sources and the specific demands of industry as either a backup power unit, for portable or transportation applications, or for running equipment independent from the conventional electricity grid.

Hydrogen releases energy when it bonds with oxygen. This can be achieved through a reaction of hydrogen in an internal combustion engine (in the place of gasoline) for automobiles (Vudumu and Koylu, 2009a) or by an electrochemical reaction in a fuel cell to produce electricity. Combustion reactions convert chemical energy into thermal energy, which can then be used to produce mechanical work and electrical energy, but fuel cells convert the chemical energy directly to electrical energy so there is less energy

lost in intermediate steps. This energy loss prevents a combustion engine from ever being as efficient as a fuel cell, but their near ubiquity in transportation could allow for early adoption of hydrogen power in that market while fuel cell alternatives are in development.

Fuel cells, as previously stated, produce power through the electrochemical reaction of hydrogen and oxygen. A typical setup places the fuel and oxidizer streams on opposite sides of a semi-permeable barrier (Figure 1.1). In the most popular type of fuel cell, Proton Exchange Membrane or Polymer Electrolyte Membrane (PEM) fuel cells, this barrier is, as its names imply, a polymer electrolyte that is permeable to protons, that is, to H^+ atoms. It is, however, impermeable to electrons. This means that electrons are compelled to travel around the membrane through wires, creating an electrical current that can be utilized.

Despite the seeming simplicity of this process, the details of a fuel cell's operational mechanism and the incurred losses are very complex and not fully understood (Biyikoglu, 2005). In order to gain insight into the fundamental processes occurring in fuel cells, many different types of models have been developed and published. Some of these are derived from first principles and some by incorporating empirical correlations with working fuel cells. Models are also of practical interest to industry, as they allow a designer to predict the behavior of fuel cells to reduce the time and expense of prototyping and testing. For industrial models, ease of use, ease of incorporation into a larger system, and an appropriate balance of comprehensiveness and computational cost are more important than a complete characterization of all aspects of the fuel cell.

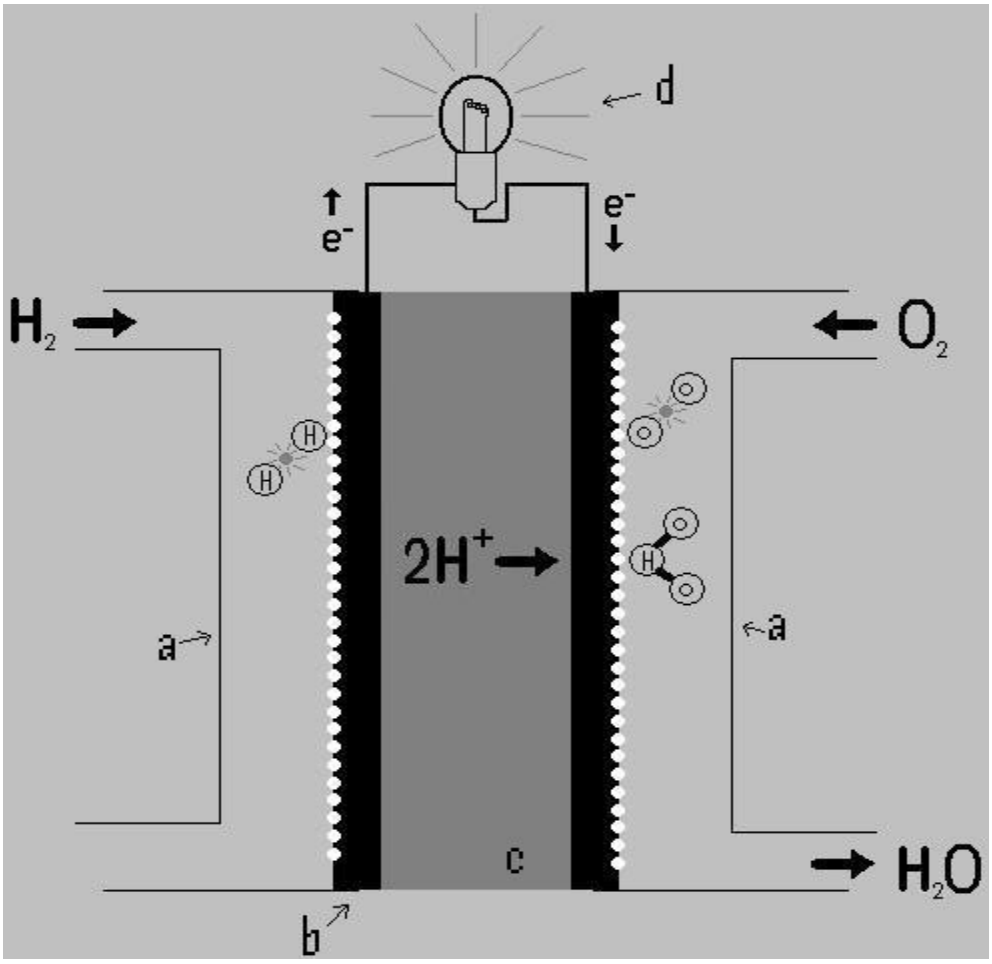

Figure 1.1. Proton exchange membrane (PEM) fuel cell: a) gas channels, b) gas diffusion layer with catalyst, c) membrane, d) external load

A model of this sort has been developed by Gamma Technologies® (GT®) (Wahiduzzaman et al., 2004). Since the GT® software package is already in use for the simulation of vehicle systems and internal combustion engines (Vudumu and Koylu, 2009a), the inclusion of a PEM model could help facilitate the incorporation of fuel cells into transportation applications. Before this can happen, however, it must be determined if the model output is consistent with working fuel cells. The model also omits the effects of humidity on a fuel cell, which is an aspect of fuel cell function that is of great concern in fuel cell systems (Buchi & Srinivasan, 1997). A functional model of humidity

dynamics should then be developed for incorporation with the current fuel cell model to increase its scope and applicability to designers of fuel cell systems.

2. LITERATURE REVIEW

2.1. INTRODUCTION

This section explains the published literature on fuel cell modeling as well as the different computational fluid dynamics software programs that have been used. The conclusion of this section will contain the objectives of this thesis.

2.2. PAST STUDIES

Much of the work in modeling PEM fuel cells has been derived from the models of Springer et al. (1991) and Bernardi and Verbrugge (1992). The Bernardi and Verbrugge model was one-dimensional, steady state, isothermal, assumed a fully hydrated membrane, and incorporated the Nernst-Planck, Schlögl's velocity, Butler-Volmer, and Stefan-Maxwell equations. The Springer et al. model was similar, but did not use porous-electrode equations and it accounted for the effects of membrane (specifically Nafion 117) water content on membrane water diffusion, electro-osmotic drag, and membrane conductivity. Membrane water content was based on its relationship to the water activity in the fuel cell as described by Zawodzinski et al. (1991).

These models were later extended by Fuller and Newman (1993) and Nguyen and White (1993) who considered flow along the channels and heat and mass transfer effects. These models, as well as those they were derived from, were valid only in the absence of liquid water. Two-phase flow was considered by Wang et al. (2001), who developed a model to predict liquid water formation and its effect on electrochemical kinetics and transport at the cathode. Further advances were made by Murgia et al. (2002), who eliminated the non-linear portions of the Bernardi and Verbrugge model, yielding a

model that was more stable and less computationally intensive. Pisani et al. (2002a) corrected for inaccuracies of the Bernardi and Verbrugge model at high current densities by taking into account the effects of water flooding in the cathode. Pisani et al. (2002b) also worked to replace as many of the fitting coefficients as possible with mechanistic derived coefficients.

Dutta et al. (2000) developed one of the first three-dimensional models by using the commercially available software package Fluent® to resolve the complete three-dimensional Navier-Stokes equations in the flow channels. Berning et al. (2002) later developed a model using the program CFX®, incorporating the effects of all major transport phenomena except water phase change. Other three-dimensional, finite element models have been made using CFD-ACE+® (Mazumder and Cole, 2003) and Star-CD® (Meng and Wang, 2004a; 2004b).

While multi-dimensional models are necessary to understand the details of fuel cell, they are nevertheless computationally demanding. Simpler quasi-dimensional models are desirable for fast computations with reasonable accuracy for practical design, control and optimization purposes. Such fuel cell simulations also provide cost-effective technical tools that considerably shorten the development time from conceptual ideas to actual products. This is especially important for PEM fuel cell technologies that are in the initial stages of development and commercialization. Hence, there is a crucial need to develop, validate and utilize simple yet predictive models for PEM fuel cells.

Wahiduzzaman et al. (2004) presented a PEM fuel cell model for the software package GT-Suite®. Although they demonstrated the model and obtained reasonable predictions, they did not validate it against experimental data. Originally, this software

has been developed to simulate internal combustion engines and has become an industry standard for many automotive companies. It has been widely used in the literature for predicting the performance of conventional gasoline and diesel engines. Very recently, its use has also been extended to successfully compute combustion and emission characteristics of hydrogen-powered engines. While this model is not as comprehensive in its formulation and omits multi-dimensional effects, its implementation in an integrated computational package allows all relevant subsystems to be simulated in the same environment, which could be attractive to industries wishing to incorporate fuel cells into designs. This is especially important for vehicles where fuel cells can power electric motors or be combined with advanced batteries.

2.3. THESIS OBJECTIVES

Based on the brief discussion above, the goal of this study is to improve and validate the initial PEM fuel cell model developed in GT-Suite® software package by Wahiduzzaman et al. (2004). In particular, its accuracy and suitability to computationally predict the operational performance of PEM fuel cells will be evaluated by comparison to the well-documented experiments in the literature. A model capable of incorporating the effects of humidity on fuel cell performance will also be developed and implemented, and the new model will also be compared with data from fuel cells available in the literature. The results presented here are expected to contribute to the improved design and analysis of PEM fuel cells and therefore lead to a faster and smoother transition to emerging cleaner and more efficient energy conversion devices in the power industry.

3. PROTON EXCHANGE MEMBRANE FUEL CELL MODEL

3.1. INTRODUCTION

In this section, the theoretical basis for the fuel cell model will be discussed. The equations that compose the stock model will be explained, and the equations used to incorporate the effects of humidity into that model will be justified. The method with which the humidity model was implemented will also be discussed in brief. The effects of the humidity model on the output of the fuel cell model will be covered in a later section.

3.2. FUEL CELL MODELING EQUATIONS AND CONSTANTS

3.2.1. Reversible Cell Voltage. The electrochemical reaction that drives a fuel cell can be expressed as Equations 1 (anode reaction) and 2 (cathode reaction), or in a combined form as Equation 3.

$$\mathbf{H_2 \rightarrow 2H^+ + 2e^-} \tag{1}$$

$$\mathbf{2H^+ + 2e^- + \frac{1}{2}O_2 \rightarrow H_2O} \tag{2}$$

$$\mathbf{H_2 + \frac{1}{2}O_2 \rightarrow H_2O} \tag{3}$$

The electrical potential of a chemical reaction is given by

$$\Delta \bar{g}_f = -nFE^o \tag{4}$$

where Δg_f is the Gibbs free energy of the reaction, n is the number of electrons transported, F is the Faraday constant, and E^o is the maximum theoretical electrical potential, or voltage. This ideal voltage is affected by both the temperature and pressure of the reaction, such that actual maximum reaction voltage is given by Equation 5,

$$E = E^o + \frac{RT}{nF} \ln \frac{\prod a_{reactants}^{v_i}}{\prod a_{products}^{v_i}} \tag{5}$$

where a is the species activity and v_i is the species stoichiometric coefficient. Gas activity is equivalent to partial pressure, and for the present calculation, the model assumes H_2O activity equals unity (liquid water). With this assumption, the reversible open circuit voltage for Equation 3 can be expressed as,

$$E = \frac{(g_f)_{H_2O} - (g_f)_{H_2} - 0.5(g_f)_{O_2}}{2F} + \frac{RT}{2F} \ln \left(p_{H_2} p_{O_2}^{\frac{1}{2}} \right) \tag{6}$$

This reversible open circuit voltage is the maximum voltage a fuel cell can produce, and the actual voltage will always be less than this maximum due to various loses, called overpotentials, in the system. In the following, three overpotentials, namely activation, ohmic, and mass transport, are discussed in detail.

3.2.2. Activation Overpotential. Activation loss is the reduction in cell electrical potential required to increase the current output of a cell beyond its output at electrochemical equilibrium. The equation used to describe the activation losses in the fuel cell model is the Tafel equation (Equation 7). The value of 2 in Equation 7 is due to

the number of charges (electrons) transfered in the hydrogen oxidation reaction (Equation 2).

$$\eta_{act} = \frac{RT}{\alpha 2F} \ln\left(\frac{i}{i_o}\right) \tag{7}$$

Equation a represents a simplification of the Butler-Volmer equation (Equation 8).

$$i = i_o \left(e^{\alpha 2F\eta_{act}/(RT)} - e^{-(1-\alpha)2F\eta_{act}/(RT)} \right) \tag{8}$$

For systems with current densities much larger than the exchange current density (when η_{act} is large), the second term in Equation 8 can be neglected, yielding

$$i = i_o e^{\alpha 2F\eta_{act}/(RT)} \tag{9}$$

which can be rewritten as Equation 7.

The exchange current density, i_o, represents the current density at electrochemical equilibrium, that is, the point at which the forward and reverse reaction rates are equal.

$$i_1 = i_2 = i_o \tag{10}$$

Forward and reverse reaction rates can be written as:

$$i_1 = 2FC_R f_1 e^{-\Delta G/(RT)} \quad (11)$$

$$i_2 = 2FC_P f_2 e^{-(\Delta G - \Delta \hat{g}_f + 2F\Delta\phi)/(RT)} \quad (12)$$

where C_P and C_R are the product and reactant concentrations, respectively, ΔG is the activation energy for the reaction, and $\Delta\phi$ is electrical potential at the reaction site. f_1 and f_2 are decay rates, and can generally be assumed equal. Setting Equations 11 and 12 equal to each other and simplifying yields the following relationship:

$$\frac{C_R}{C_P} = e^{(\Delta \hat{g}_f - 2F\Delta\phi)/(RT)} \quad (13)$$

Since $\Delta \hat{g}_f$, $2F$, and R are constant, for a given temperature we can say that i_o occurs when the electrical potential at the reaction site is proportional to chemical potential:

$$\Delta\phi \sim \ln\left(\frac{C_R}{C_P}\right) \quad (14)$$

Typical values for i_o for PEM fuel cells are on the order of 10^{-4} mA/cm^2. The operational range of fuel cells is generally many orders of magnitude larger, validating the simplification of the Butler-Volmer equation (Equation 9).

The constant α in Equation 7, the charge transfer coefficient, describes the asymmetry in activation energy in an electrochemical reaction. Values of α range between 0 and 1, with 0.5 representing a symmetric reaction, that is, when the increase in

activation energy for the reverse reaction is equivalent to the decrease in activation energy for the forward reaction. In a fuel cell, α will vary based on type and quantity of catalyst used, and generally has a value between 0.2 and 0.5.

3.2.3. Ohmic Overpotential. Moving charged particles incurs losses, and these losses in a fuel cell are referred to as the ohmic overpotential, η_{ohm}. Of the two charged particles transferred in a PEM fuel cell system, protons and electrons, the hydrogen ion transport through the electrolyte accounts for the majority of the resistance. In conducting metals, valence electrons are relatively free to move about the material; in order for ions to move through a material, they must take advantage of free spaces in the physical structure of the electrolyte—vacancies and interstitial sites in ceramics or charged sites in polymers. Ions can also be transported by associating with molecules in a liquid, for example H_3O^+. In any case, charge conductivity is much less for ions than for electrons, and so electrical resistance can be ignored.

The voltage drop due to ion transport resistance then follows Ohm's law:

$$\eta_{ohm} = IR_i \tag{15}$$

which can be written in terms of current density as

$$\eta_{ohm} = iAR_i \tag{16}$$

3.2.4. Mass Transport Overpotential. The physical limits of mass transport rate impose two modes of voltage loss on a fuel cell—decreased Nernst voltage and reaction rate. These will both decrease as reactant concentrations at the reaction site fall away from the bulk flow concentration. The linear concentration gradient that develops can be described by the flux of the reactants, J , as

$$J = -D^{eff}\frac{C_R - C_R^o}{\delta} \tag{17}$$

where C_R^o is the reactant concentration in the bulk flow, D^{eff} is the effective diffusivity through the diffusion layer, and δ is the diffusion layer thickness. At steady state, reactant flux through the diffusion layer will equal reactant consumption so that:

$$i = 4FJ \tag{18}$$

The numerical coefficient in Equation 18 is 4 as opposed to 2 because here oxygen is being considered, not hydrogen, and there are four charged particles transferred per O_2 molecule. Since D^{eff} of oxygen is much less than that of hydrogen, the mass transport loses of hydrogen can be neglected.

Combining Equations 17 and 18 gives a relationship between reaction concentrations and current density (Equation 19). From this, the maximum possible current density, when the current density is limited by the diffusivity of the reactant gas and diffusion layer thickness, can be calculated by setting C_R, the reactant concentration

at the reactant site, equal to zero (Equation 20). This is the limiting current density, or the maximum possible current density of the cell, and is denoted i_l.

$$i = 4FD\frac{C_R^o - C_R}{\delta} \tag{19}$$

$$i_l = 4FD\frac{C_R^o}{\delta} \tag{20}$$

The decrease in voltage due to mass transport inefficiencies can be expressed in terms of limiting current density. The concentration losses resulting from reduced Nernst voltage can be written as the change in Equation 5 due to reduced reactant concentration.

$$\eta_{mt,nernst} = \left(E^o + \frac{RT}{nF}\ln C_R^o\right) - \left(E^o + \frac{RT}{nF}\ln C_R\right) = \frac{RT}{nF}\ln\frac{C_R^o}{C_R} \tag{21}$$

Equation 21 can be combined with Equations 19 and 20 to find the voltage loss in terms of current density and limiting current density.

$$\eta_{mt,nernst} = -\frac{RT}{nF}\ln\left(1 - \frac{i}{i_l}\right) \tag{22}$$

In order to account for the reduction in reaction rate due to reactant concentration, one must rewrite Equation 9 in an alternate format—one that takes into account species concentration.

$$i = i_o\left(\frac{C_R^*}{C_R^o}e^{\alpha 2F\eta_{act}/(RT)}\right) \tag{23}$$

Rearranging to get Equation w in terms of voltage loss,

$$\eta_{act} = \frac{RT}{\alpha n F} \ln\left(\frac{i C_R^o}{i_o C_R^*}\right) \tag{24}$$

where C_R^* is an arbitrary reactant concentration. The bulk and actual reactant concentrations can be substituted in for C_R^* and subtracted to find the reduction in voltage.

$$\eta_{mt,act} = \frac{RT}{\alpha n F} \ln\left(\frac{i C_R^o}{i_o C_R}\right) - \frac{RT}{\alpha n F} \ln\left(\frac{i C_R^o}{i_o C_R^o}\right) = \frac{RT}{\alpha n F} \ln\left(\frac{C_R^o}{C_R}\right) \tag{25}$$

Equation 25 can be rewritten in terms of limiting current density, just as Equation 21 was.

$$\eta_{mt,act} = -\frac{RT}{\alpha n F} \ln\left(1 - \frac{i}{i_l}\right) \tag{26}$$

Equations 22 and 26 can be combined to give an expression for the total theoretical overpotential resulting from mass transport limitations.

$$\eta_{mt} = -\frac{RT}{nF} \ln\left(1 - \frac{i}{i_l}\right) - \frac{RT}{\alpha n F} \ln\left(1 - \frac{i}{i_l}\right) = -\frac{RT}{nF}\left(1 + \frac{1}{\alpha}\right) \ln\left(1 - \frac{i}{i_l}\right) \tag{27}$$

Real fuel cell mass transport losses are often under predicted by Equation 27, and so the equation generally used is:

$$\eta_{mt} = -C \ln\left(1 - \frac{i}{i_l}\right) \tag{28}$$

Here C is an empirical coefficient that is referred to as the mass transport loss coefficient.

3.2.5. Fuel Cell Voltage. The actual voltage output of a fuel cell can be modeled by subtracting the overpotentials from the reversible fuel cell voltage.

$$V_{cell} = E - \eta_{act} - \eta_{ohm} - \eta_{mt} \tag{29}$$

Substituting Equations 6, 7, 16, and 28 into Equation 29, the real voltage output of the fuel cell is then written as

$$V_{cell} = \frac{(\hat{g}_f)_{H_2O} - (\hat{g}_f)_{H_2} - 0.5(\hat{g}_f)_{O_2}}{2F} + \frac{RT}{2F}\ln\left(p_{H_2} p_{O_2}^{\frac{1}{2}}\right) - \frac{RT}{\alpha 2F}\ln\left(\frac{i}{i_o}\right) - iAR_i + C\ln\left(1 - \frac{i}{i_l}\right) \tag{30}$$

Values from Equation 30 that are variables in the software model are given in Table 3.1.

Table 3.1. Fuel cell model parameters

Symbol	Term	Units
i_o	Exchange Current Density	mA/cm^2
α	Charge Transport Coefficient	
R_i	Ionic Resistance	Ω
A	Cell Active Surface Area	cm^2
i_l	Limiting Current Density	mA/cm^2
C	Mass Transport Loss Coefficient	V

3.3. THERMAL MODEL

The temperature of the fuel cell stack is determined through a simple heat transfer analysis. The thermal energy generated by the stack is transferred without loss to masses of defined properties. Heat is then dissipated to the environment through convection to a constant temperature fluid.

The amount of thermal energy produced by the fuel cell model is equal to the difference between the ideal power generation of the stack and the actual (Zeman, 2010). This is illustrated in Figure 3.1, where $\dot{Q}$ is the amount of thermal energy transferred to the mass per unit time (Equation 31).

$$\dot{Q} = P^{\bullet} - P = IE^{o} - IV_{cell} \tag{31}$$

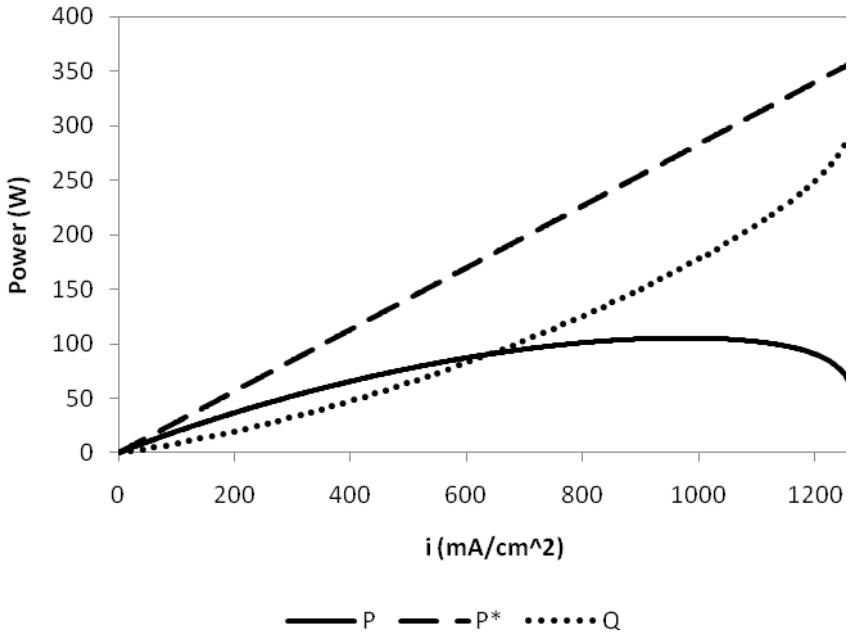

Figure 3.1. Fuel cell stack power output (P), ideal power output (P*), and thermal output (Q)

3.4. HUMIDITY MODEL

3.4.1. Modeling Equations. Water content of the fuel cell was determined on a rate basis; water flow rate into the fuel cell with the reactant gasses and water production rate by the cell. Correlations for the effect of humidity on fuel cell properties have been taken from the literature. This section outlines the theoretical basis and modeling equations used to calculate the effect of humidity, changes in temperature, and reactant concentrations on a fuel cell.

3.4.1.1. Water activity. Water activity in the fuel cell was determined from first principles. Since the fuel cell model was quasi-one-dimensional, humidity distribution was ignored and average water activity was calculated.

Water activity is defined as,

$$a \equiv \frac{m_{H_2O}}{m_{H_2O}^{sat}} \tag{32}$$

where m_{H_2O} is the mass of water in the environment and $m_{H_2O}^{sat}$ is the mass of water vapor at saturation. For values of $a \leq 1$, water activity is synonymous with relative humidity.

Calculating water activity inside the fuel cell stack begins with a determination of the saturated vapor pressure of the fuel and oxidizer gas streams. This is given in Equation 33, from (Maggio et al. 2001):

$$P_{H_2O_i}^{sat} = 101{,}325e^{\left(13.669 - \frac{5096.2a}{T_i}\right)} \tag{33}$$

where T_i is the average temperature of the inflow gases. The partial pressure of water in the inflow gases is then:

$$P_{H_2O_i} = \phi P_{H_2O_i}^{sat} \tag{34}$$

where ϕ is the average relative humidity of inflow gases. The total molar flow rate of water into the fuel cell is calculated by assuming that water vapor is an ideal gas, that is,

$$\dot{n}_{H_2O,in} = \frac{P_{H_2O_i}\dot{V}}{RT_i} \tag{35}$$

and the total molar flow rate of non-vapor gases into the fuel cell is,

$$\dot{n}_{gas,in} = \frac{\left(P_{avg} - P_{H_2O_i}\right)\dot{V}}{RT_i} \tag{36}$$

where P_{avg} is the average of the cathode and anode pressures and $\dot{V}$ is the sum of the cathode and anode gas flow rates.

Besides the water brought in to the cell by the fuel and oxidizer streams, there is water produced by the cell's driving electrochemical reaction (Equation 3). This is related to the current output of the fuel cell, as each electron produced corresponds to half of a water molecule produced from the hydrogen oxidation reaction. This "half" value is taken into account by the value of 2 in Equation 37. Faraday's constant, F , converts the charge per second given by the current into moles per second.

$$\dot{n}_{H_2O,prod} = \frac{I}{2F} \tag{37}$$

From Equations 35, 36, 37, and the average of the cathode and anode pressures, the water vapor pressure at the outlet of the cell can be calculated.

$$P_{H_2O} = \left(\frac{\dot{n}_{H_2O,in} + \dot{n}_{H_2O,prod}}{\dot{n}_{gas,in} + \dot{n}_{H_2O,in} + \dot{n}_{H_2O,prod}}\right)P_{avg} \tag{38}$$

The average water activity in the cell (Equation 39) can be found, using Equation 40 for the saturation pressure of water inside the fuel cell.

$$a_{avg} = \frac{P_{H_2O,avg}}{P^{sat}_{H_2O}} = \frac{P_{H_2O_i} + P_{H_2O}}{2 * P^{sat}_{H_2O}} \quad (39)$$

$$P^{sat}_{H_2O} = 101{,}325e^{\left(13.669 - \frac{5096.23}{T}\right)} \quad (40)$$

Here T is the fuel cell temperature.

3.4.1.2. Membrane resistance. The model used to take into account the effects of water activity on membrane resistance was based on the work by Springer et al. (1991). Figure 3.2 shows the relationship between water vapor activity in the environment and water content of the membrane at 303 K. Water content of the membrane is defined as the number of molecules of water per sulfonic acid $(SO_3^- H^+)$ site in the membrane.

The relationship between a_{avg} and λ_{303} is a piecewise function given by Equations 41 and 42.

$$\lambda_{303} = 0.043 + 17.81a_{avg} - 39.85{a_{avg}}^2 + 36.0{a_{avg}}^3 \text{ for } 0 < a_{avg} \leq 1 \quad (41)$$

$$\lambda_{303} = 14 + 1.4(a_{avg} - 1) \text{ for } 1 \leq a_{avg} \leq 3 \quad (42)$$

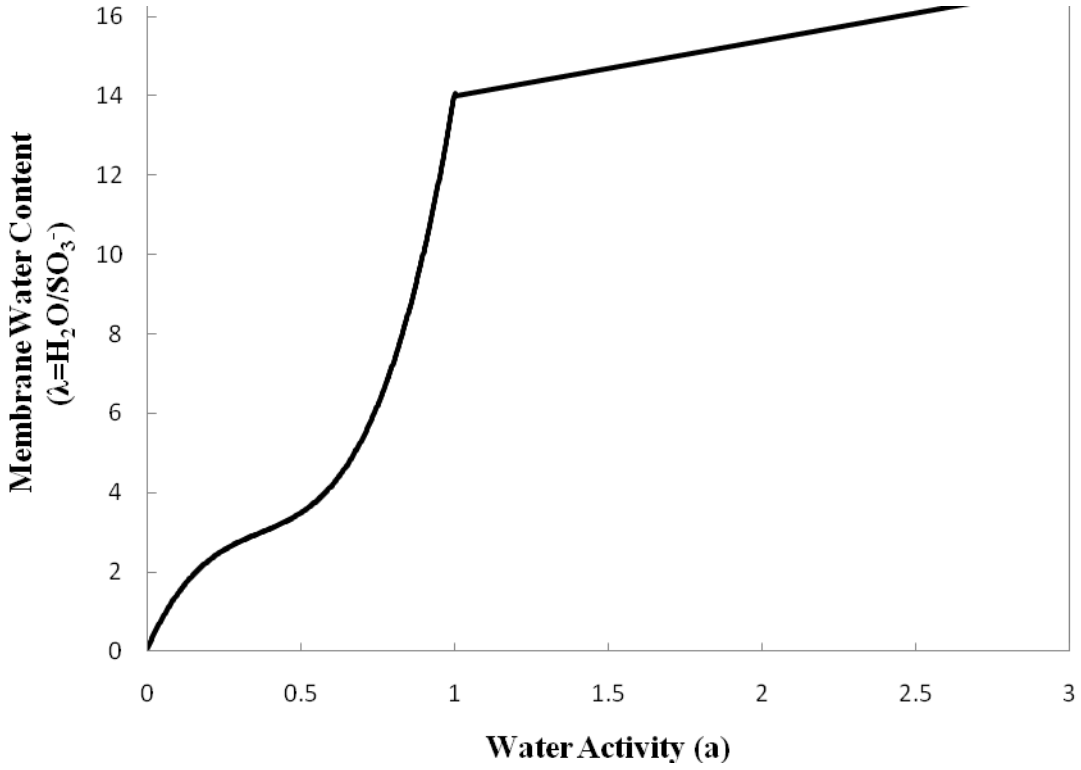

Figure 3.2. Relationship between water vapor activity and membrane water content at 303 K (from Springer et al., 1991)

For $\lambda > 1$, water content was related to membrane conductivity (Springer et al., 1991) as:

$$\sigma_{30a} = 0.005193\lambda_{30a} - 0.00326 \quad \text{for } \lambda > 1 \tag{43}$$

and correlated to temperature change by,

$$\sigma = \sigma_{30a} e^{\left[1268\left(\frac{1}{303} - \frac{1}{T}\right)\right]} \tag{44}$$

Membrane resistance is related to conductivity by the definition:

$$\Omega \equiv \frac{d}{A\sigma} \tag{45}$$

3.4.1.3. Limiting current density. The limiting current density of the fuel cell, i_ℓ, is also affected by the relative humidity of the inflow gasses. As water content of the cathode gases increases, the bulk concentration of oxygen is decreased. For the reasons given in the discussion of mass transport overpotential, Section 3.2.4, oxygen only is considered here, and the effect of hydrogen concentration on the limiting current density is assumed to be negligible. Limiting current density is related to bulk concentration by Equation 46.

$$i_\ell = 4FD^{eff}\left(\frac{C_R^o}{\delta}\right) \tag{46}$$

D^{eff} is the effective diffusivity of the oxygen in the gas diffusion layer, and it is proportional to the bulk diffusivity, D_{AB}, but modified by the geometry of the diffusion layer. The temperature and pressure dependence of D_{AB} has been given by Fuller et al. (1966) as,

$$D_{AB} = \frac{10^{-3}T^{\frac{7}{4}}\left(\frac{1}{M_A}+\frac{1}{M_B}\right)^2}{P\left[\left(\Sigma_A v_i\right)^{1/3}+\left(\Sigma_B v_i\right)^{1/3}\right]^2} \tag{47}$$

From this, the percent change in diffusivity due to a temperature and pressure change from reference values is given by:

$$\frac{D_{AB(T,P)} - D_{AB(T_{ref},P_{ref})}}{D_{AB(T_{ref},P_{ref})}} = \left(\frac{T}{T_{ref}}\right)^{\frac{7}{4}}\left(\frac{P_{ref}}{P}\right) - 1 \tag{48}$$

Consequently, given a reference effective diffusivity at a known temperature and pressure, the effective diffusivity at any temperature and pressure can be found.

$$D^{eff} = \left(\frac{T}{T_{ref}}\right)^{\frac{7}{4}}\left(\frac{P_{ref}}{P}\right)D^{eff}_{(T_{ref},P_{ref})} \tag{49}$$

δ in Equation 46 is the diffusion layer thickness, and the value of 4 represents the number of charged particles transferred in the cell per O_2 molecule. The bulk concentration, $\overline{C_R^o}$, can be derived from a ratio of the molar and volumetric flow rates of oxygen.

$$\overline{C_R^o} = \frac{\dot{n}_{O_2}}{\dot{V}} = X_{O_2 i}\frac{\dot{n}_{gas}}{\dot{V}} \tag{50}$$

where $X_{O_2 i}$ is the mole fraction of dry inflow gas, and,

$$\frac{\dot{n}_{gas}}{\dot{V}} = \frac{\left(P_{cath} - P_{H_2O,avg}\right)}{RT} \tag{51}$$

The accumulation of liquid water in the gas diffusion layer and the subsequent reduction in effective diffusivity was not considered here. It is assumed that, for relative humidity levels under 100%, gas diffusion layer saturation is negligible (Dawes et al., 2009). Operation of a fuel cell near, at, or above 100% relative humidity for any length of time is not advised, as liquid water blocks catalyst sites and reduces the effective porosity of the gas diffusion layer (Yamada et al., 2006).

3.4.1.4. Reactant mole fraction. The reactant concentration in the humidified anode and cathode streams must also be calculated for determination of the Nernst voltage (Equation 6). The values of the average oxygen and hydrogen mole fractions are given in Equations 52 and 53, respectively.

$$X_{O_2} = X_{O_2 i}\left(1 - \frac{P_{H_2O,avg}}{P_{cath}}\right) \tag{52}$$

$$X_{H_2} = X_{H_2 i}\left(1 - \frac{P_{H_2O,avg}}{P_{anode}}\right) \tag{53}$$

This effect on the Nernst voltage is distinct from the effect given by Equation 22; Equations 52 and 53 account for a change in open circuit voltage caused by a reduction in bulk concentration, whereas Equation 22 accounts for a reduction in voltage due to reduced local reactant concentration at high current densities.

3.4.1.5. Exchange current density. The change in exchange current density, i_o, with temperature was noted by Rajani and Kolar (2007), who described the relationship as,

$$i_{o(T)} = i_{o(T_{ref})} e^{\left[\frac{\Delta E}{R}\left(\frac{1}{T_{ref}} - \frac{1}{T}\right)\right]} \quad (54)$$

where ΔE is the reaction activation energy and has a value of 72,000 (J/mol) and T_{ref} is the reference temperature from Equation 48.

3.4.2. Implementation. Incorporation of humidity dynamics into the fuel cell model was achieved through a calculation loop external to the fuel cell model. Figure 3.3 shows the complete setup, and Figures 3.4-3.6 show the humidity calculating portion in detail. Values output by the fuel cell model, namely temperature and current, were accepted as inputs and the humidity equations output membrane resistance, limiting current density, and reactant mole fractions for use by the fuel cell model. The values were returned to the fuel cell model by first recording them as a Results Variable (RLT), then by reading those values with an RLTDependence—a dependent variable that takes its value from its an RLT. The parameters in the fuel cell model were then set to read their associated RLTDependence. Since the RLTDependences require an initial output value, the fuel cell power request was delayed by ten times the RLT sample rate. This allows a true calculated output value to be determined before fuel cell operations begin.

New parameters introduced by the humidity modeling equations that are required to be specified by the user are listed in Table 3.2.

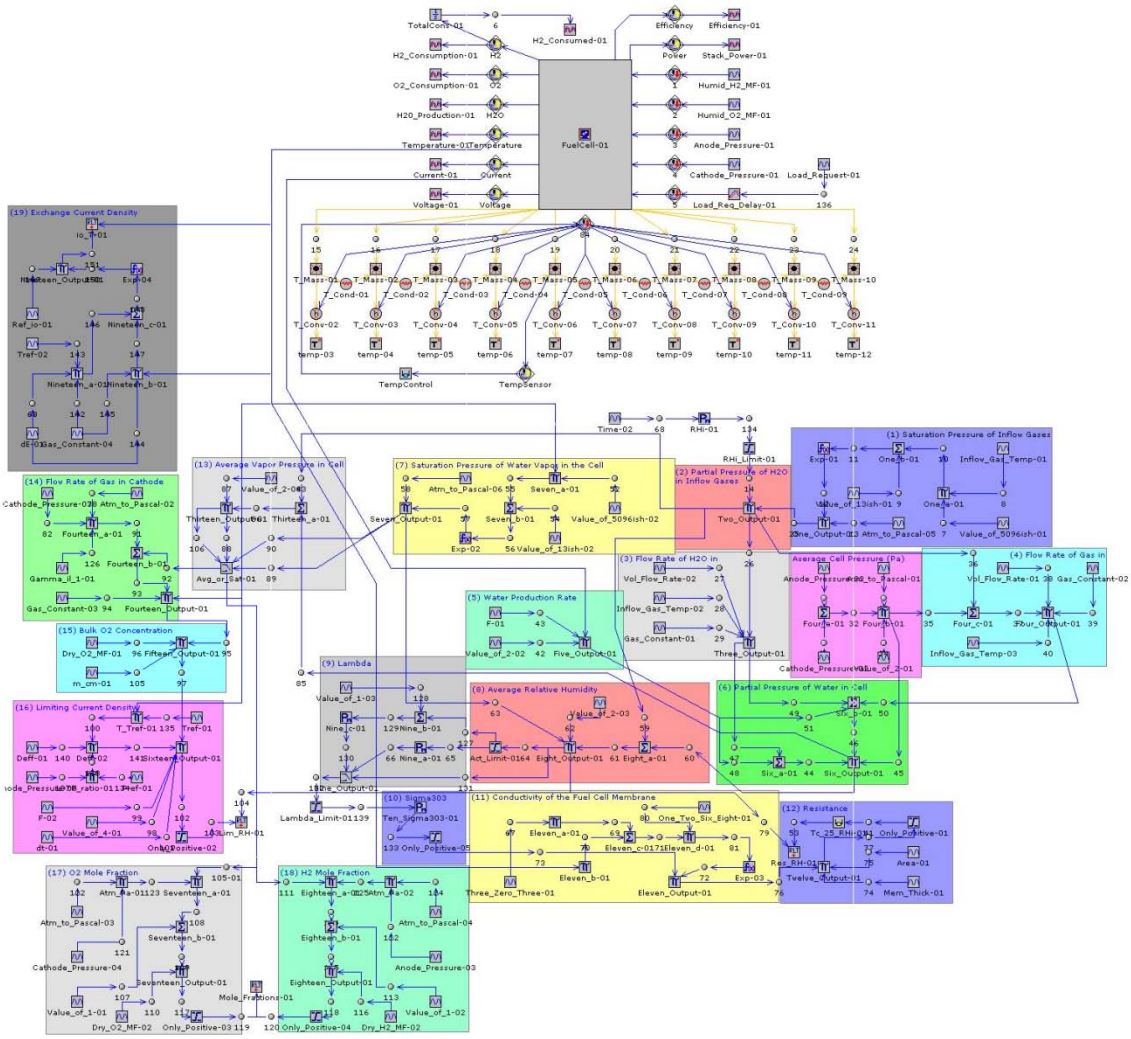

Figure 3.3. Fuel cell humidity model implemented in GT-Suite®

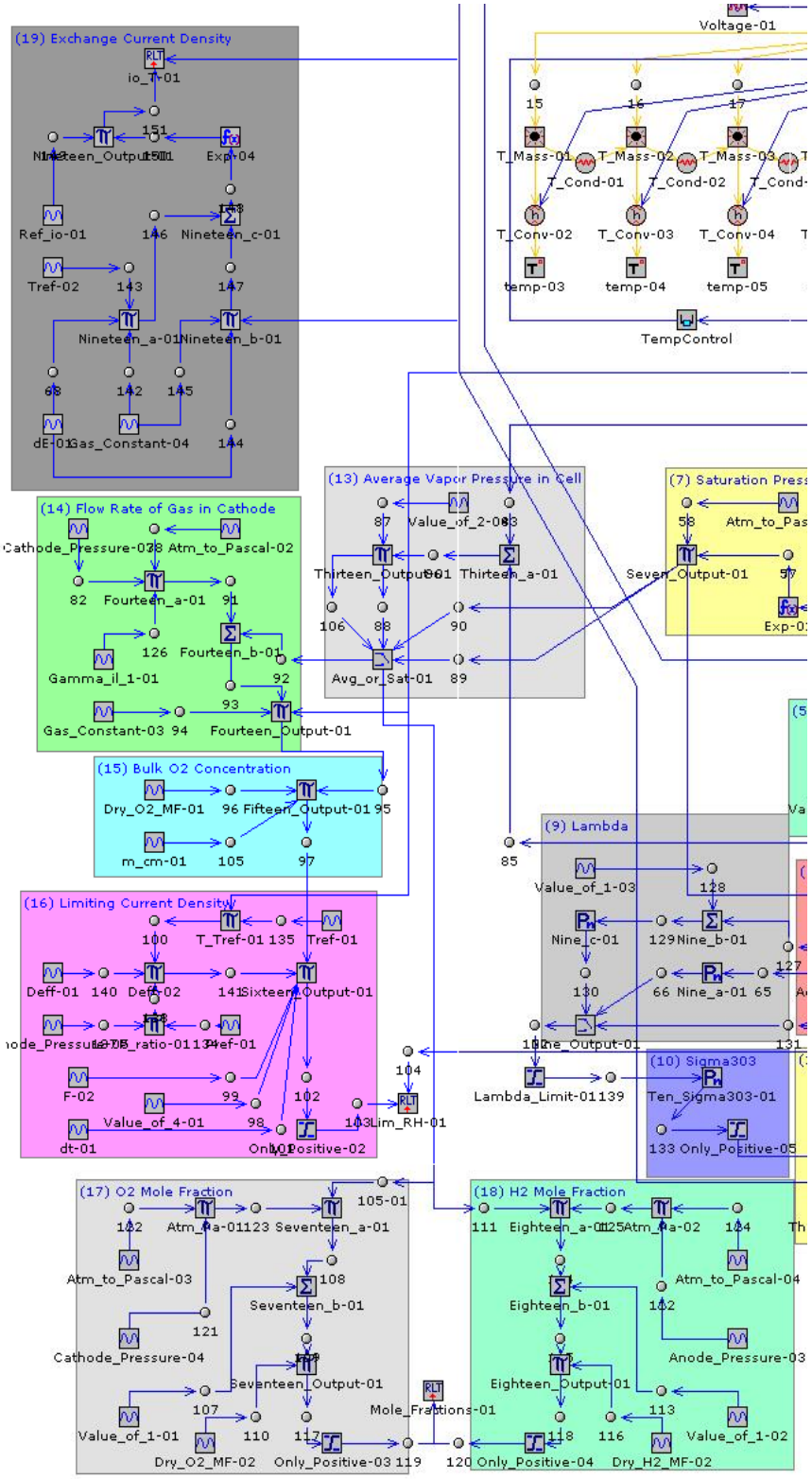

Figure 3.4. Detail from Figure 3.3, left

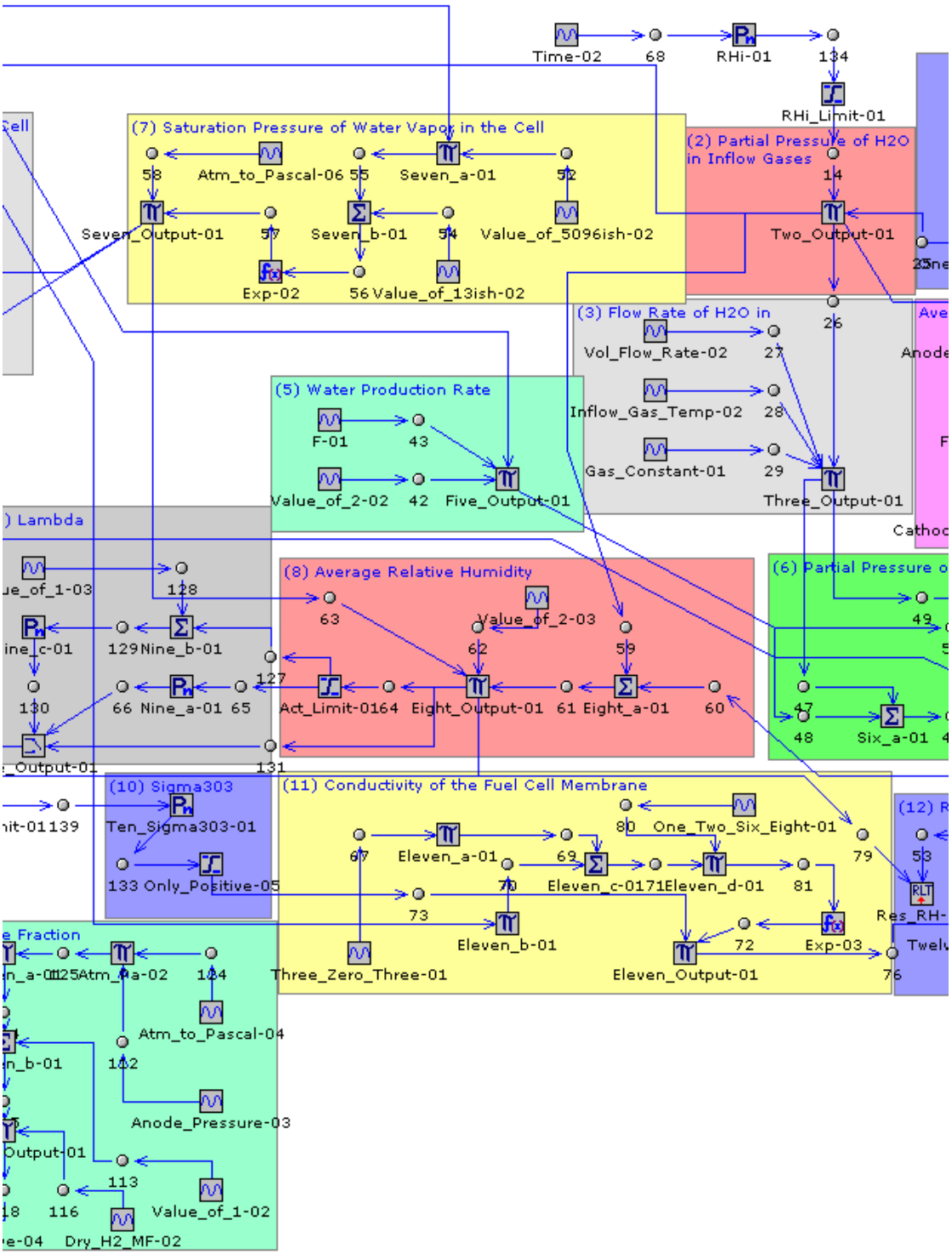

Figure 3.5. Detail from Figure 3.3, middle. With this configuration, the relative humidity of the inflow gases is variable with time

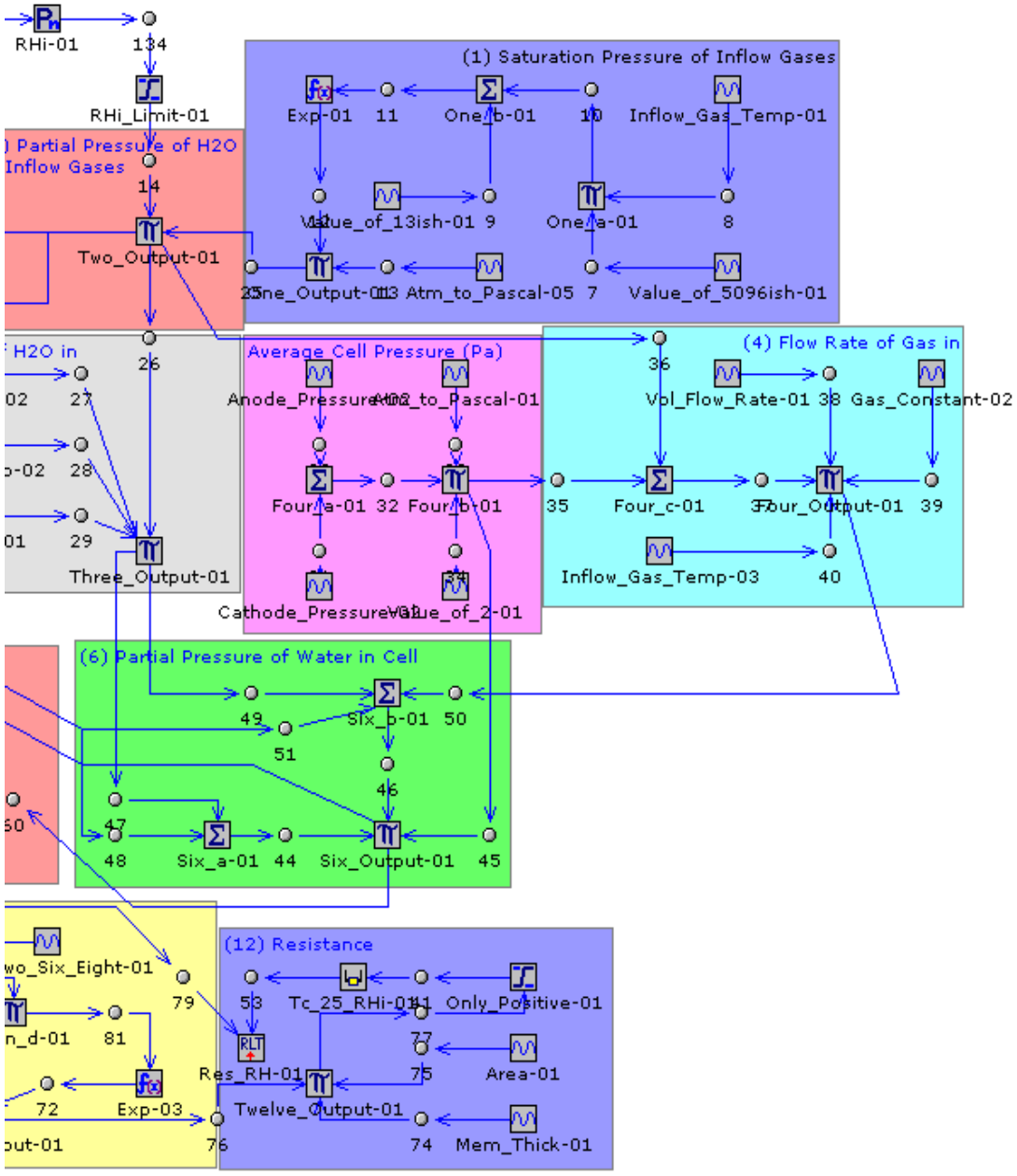

Figure 3.6. Detail from Figure 3.3, right

Table 3.2. New user input parameters for the humidity model

Symbol	Description	Units
P_{cath}	Pressure of cathode chamber	Pa
P_{anode}	Pressure of anode chamber	Pa
ϕ	Relative humidity of the inlet stream	-
$\dot{V}$	Total (sum) volumetric flow rate of the fuel and oxidizer streams	m^3/s
T_i	Temperature in the inlet stream	K
T_{ref}	Reference temperature at which the FC was modeled	K
$X_{O_2 i}$	Mole fraction of oxygen in the dry stream	-
$X_{H_2 i}$	Mole fraction of hydrogen in the dry stream	-
d	Membrane thickness	cm
A	Fuel cell active surface area	cm^2
D_{ref}^{eff}	Effective diffusivity of oxygen through the gas diffusion layer	cm^2/s
δ	Thickness of the gas diffusion layer	cm

4. RESULTS AND DISCUSSION

4.1. INTRODUCTION

This section begins by discussing the significance of the polarization curve and what effect different modeling parameters and their associated physical phenomena have on that curve. The ability of the standard model to reproduce a fuel cell and its predictive capabilities are then explored. Finally, the fuel cell model with the additional relationships discussed in Section 3.4 is compared with experimental data.

4.2. TEST PROCEDURES

It cannot be assumed that all parameters of the fuel cell model will be known; C , the mass transport loss coefficient, is a purely empirical value and other parameters, such as the limiting current density, i_l, are dependent on many disparate factors (gas diffusion layer mesh type, initial pore size, and percent compression for i_l) and so cannot easily be determined theoretically and may be difficult to measure in situ. Because of this, the values of the parameters are found by reproducing the polarization curve of the fuel cell to be modeled.

The polarization curve of a fuel cell is a plot of how the voltage varies over its range of current outputs (Figure 4.1). The three overpotentials (Equations 7, 16, and 28) dominate different regions of the polarization curve, as can be seen in Figure 4.2—the activation overpotential predominates in the low current density region, mass transport losses have their greatest impact at high current densities, and ohmic losses increase proportionally with increasing current density. The effect of the overpotentials can be

deconstructed further with an analysis of the effects of changes in individual parameters. Figures 4.3 through 4.7 show the change in fuel cell performance resulting from variation in a single parameter. With an understanding of this, it is possible to qualitatively replicate a polarization curve and therefore model the fuel cell that produces the polarization curve.

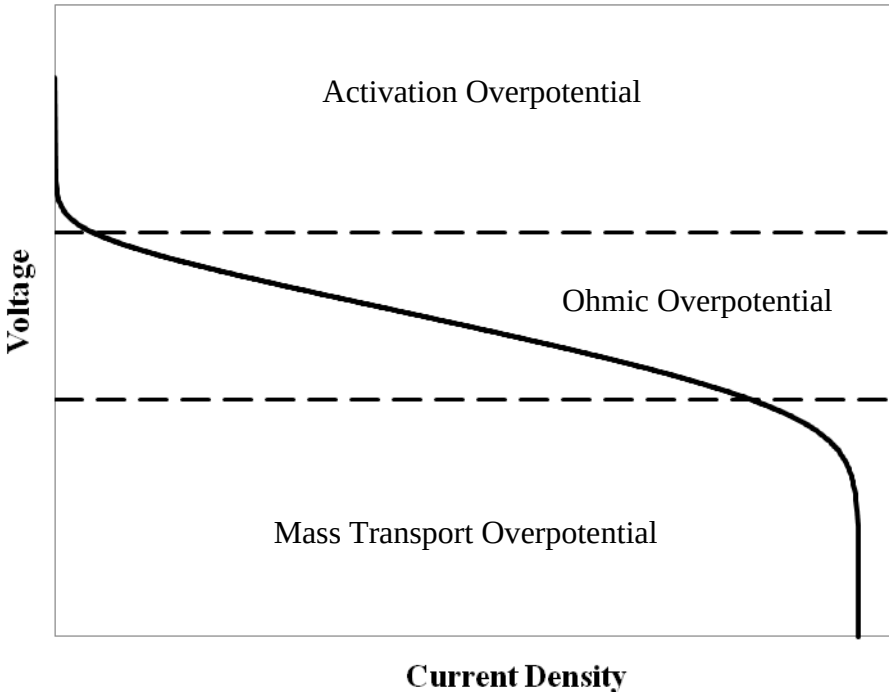

Figure 4.1. A generic polarization curve showing the overpotential regions

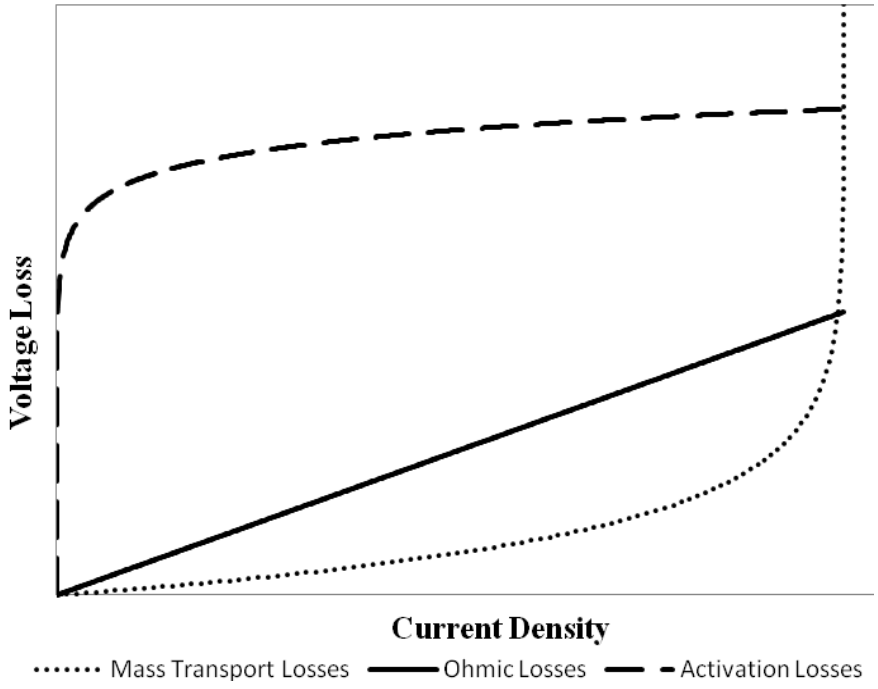

Figure 4.2. Voltage losses contributing to a polarization curve

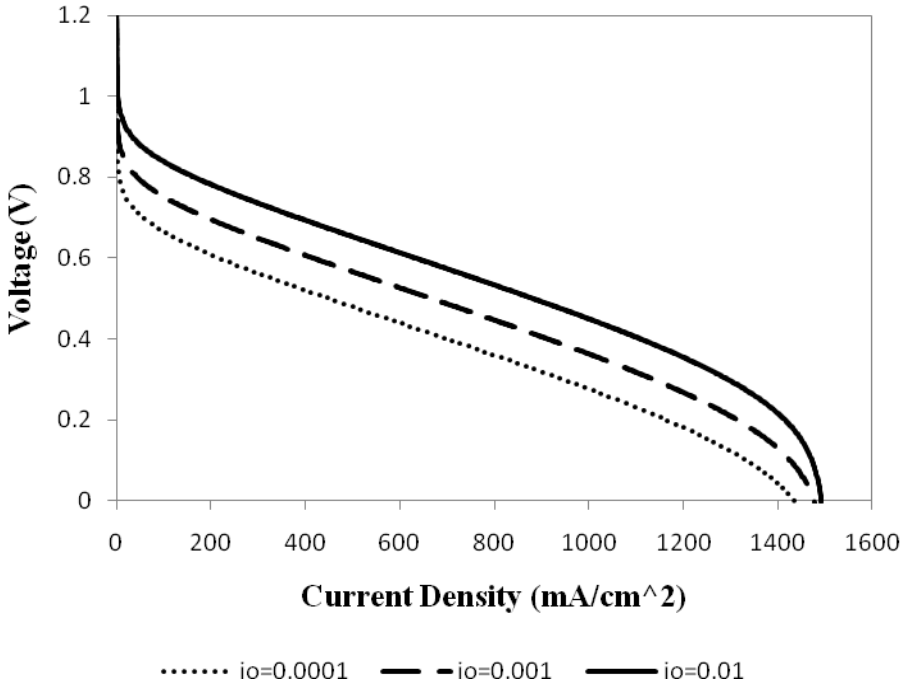

Figure 4.3. Variable exchange current density (mA/cm^2)

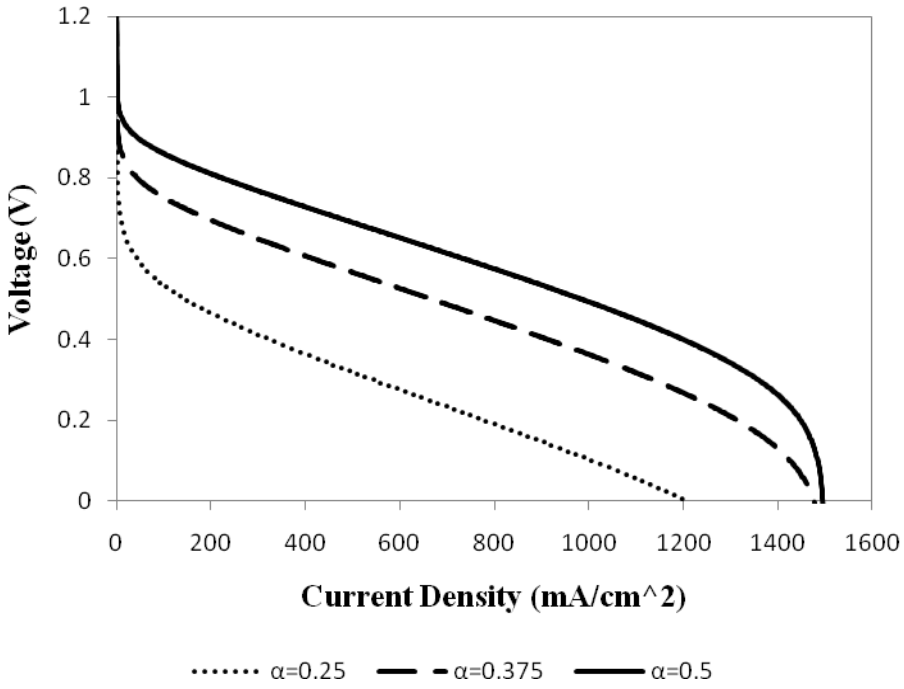

Figure 4.4. Variable charge transfer coefficient

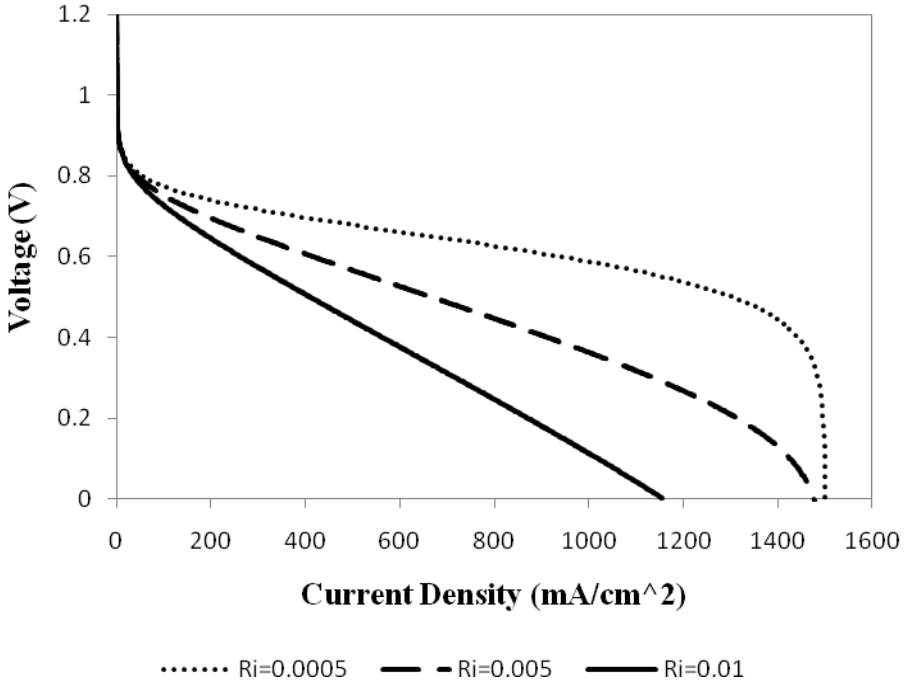

Figure 4.5. Variable membrane resistance (Ω)

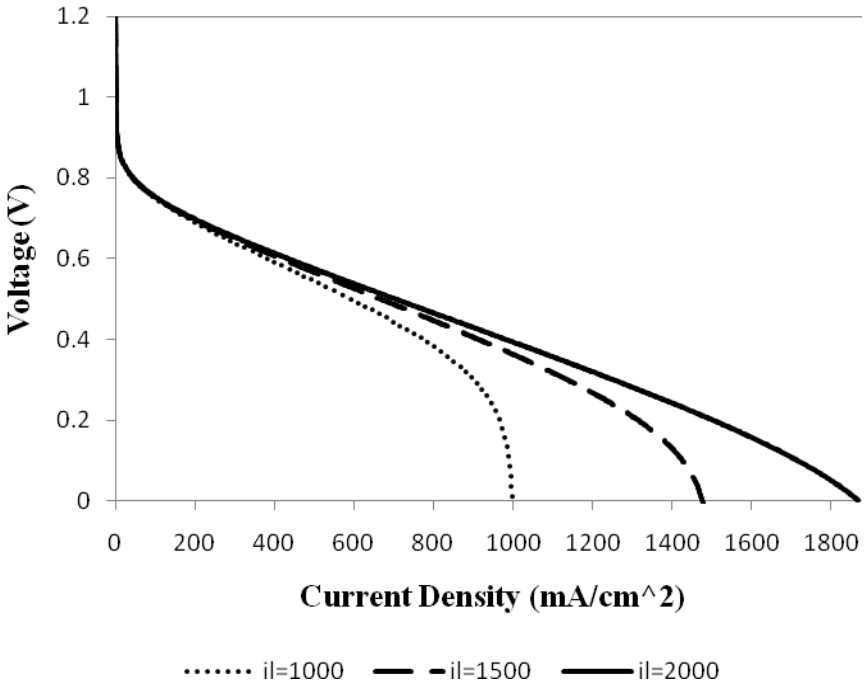

Figure 4.6. Variable limiting current density (mA/cm^2)

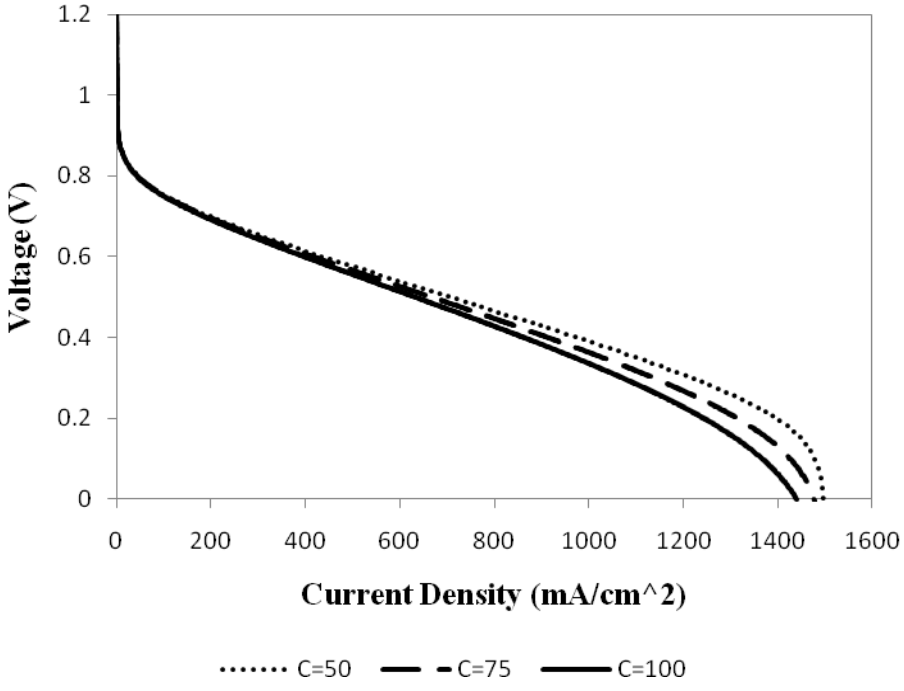

Figure 4.7. Variable mass transport loss coefficient (mV)

4.3. VALIDATION OF NON-HUMID PEM FUEL CELL MODEL

The first direct comparison of the non-humid fuel cell model under consideration here was performed against data presented by Fontes et al. (2007). The Fontes model was presented alongside values derived from the fuel cell against which they tested their model. From these values, it was possible to derive the parameters used by the model in the present study to define a fuel cell's performance. This allowed it to be seen if the model was capable of reproducing data without using the parameters as "fitting coefficients," chosen specifically to reproduce a polarization curve (Pisani et al., 2002b). A comparison between the two data sets is given in Figure 4.8. Values for the modeling parameters are listed in Table 4.1.

These results give confidence that the model output is a reliable interpretation of its input parameters and that, for a set of parameters, it is consistent with fuel cell performance in the literature. This also implies that, inversely, when a polarization curve is copied with parameters used as fitting coefficients, these parameters are meaningful with respect to the electrochemical theory (Section 3.2) and not arbitrary.

This was confirmed with a comparison to the model results given in O'Hayre et al. (2007) (Figure 4.9). In that study, mass transport loses were considered differently than they have been here, and so values for i_l and C were not derivable from reported modeling parameters. In lieu of this, these parameters were used as fitting coefficients; values were selected such that the performance of the model discussed here matched that of the O'Hayre model. This served to confirm that the mass transport modeling equation (Equation 28) gives a polarization curve contour consistent with that of models reported in the literature.

The next comparison made was with a study by Ersoz et al. (2006). In that study, a fuel cell system was modeled and the efficiency for a variety of fuel cell stack sizes was reported. Since only the number of cells in the fuel cell stack changed, the voltage/current response (the polarization curve) for each cell did not change, but the current and voltage output needed by each stack size to meet the requested power output (constant for all stack sizes) did change, as illustrated by Figure 4.10. This allowed this study's calculations of efficiency for various points on the polarization curve to be compared. The results of this can be seen in Table 4.2, and show good correlation with the values derived by Ersoz et al. This shows that the model's calculation of efficiency, and hence of the rate of energy transferred to the thermal model, is accurate.

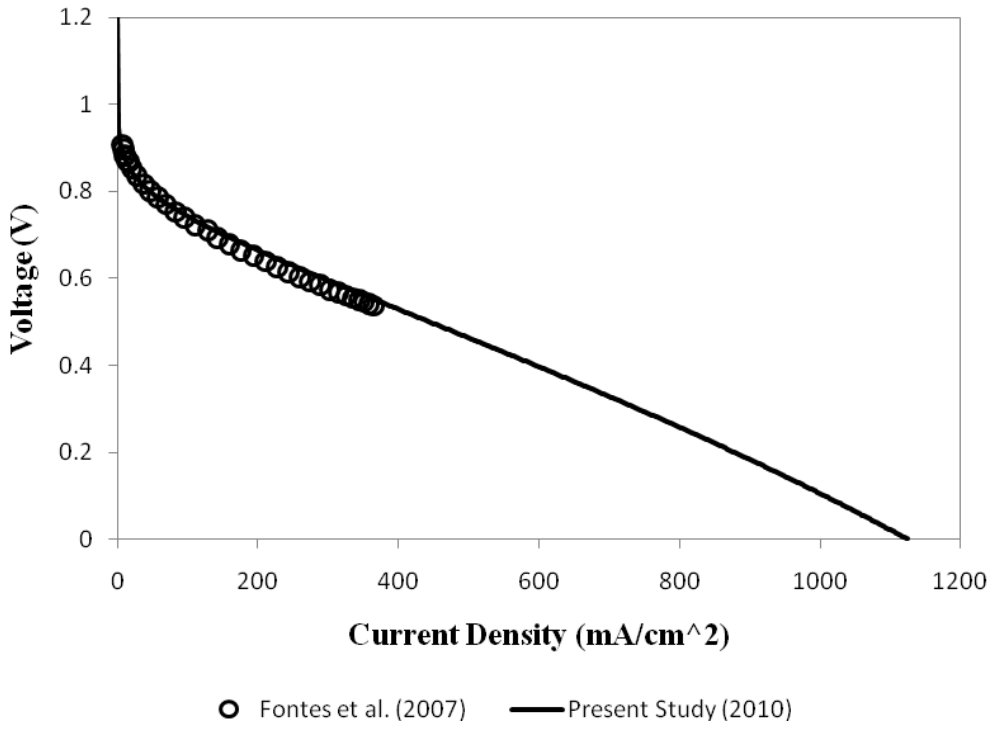

Figure 4.8. Comparison of fuel cell outputs given by Fontes et al. (2007) and the present study's model

Table 4.1. Modeling parameters given by Fontes et al. (2007)

Parameter	Value	Units
i_o	0.00234	mA/cm^2
i_l	2000	mA/cm^2
R_i	0.0041	Ω
α	0.35	
C	0.562	V

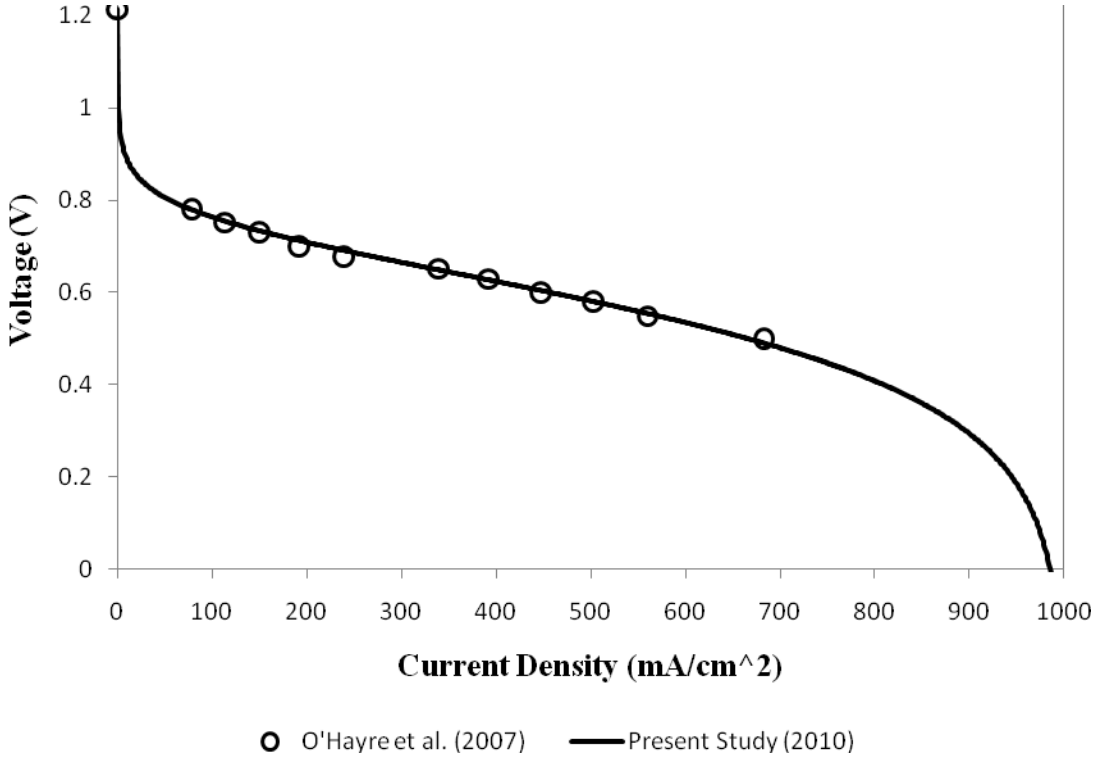

Figure 4.9. Copied polarization curve from O'Hayre et al. (2007)

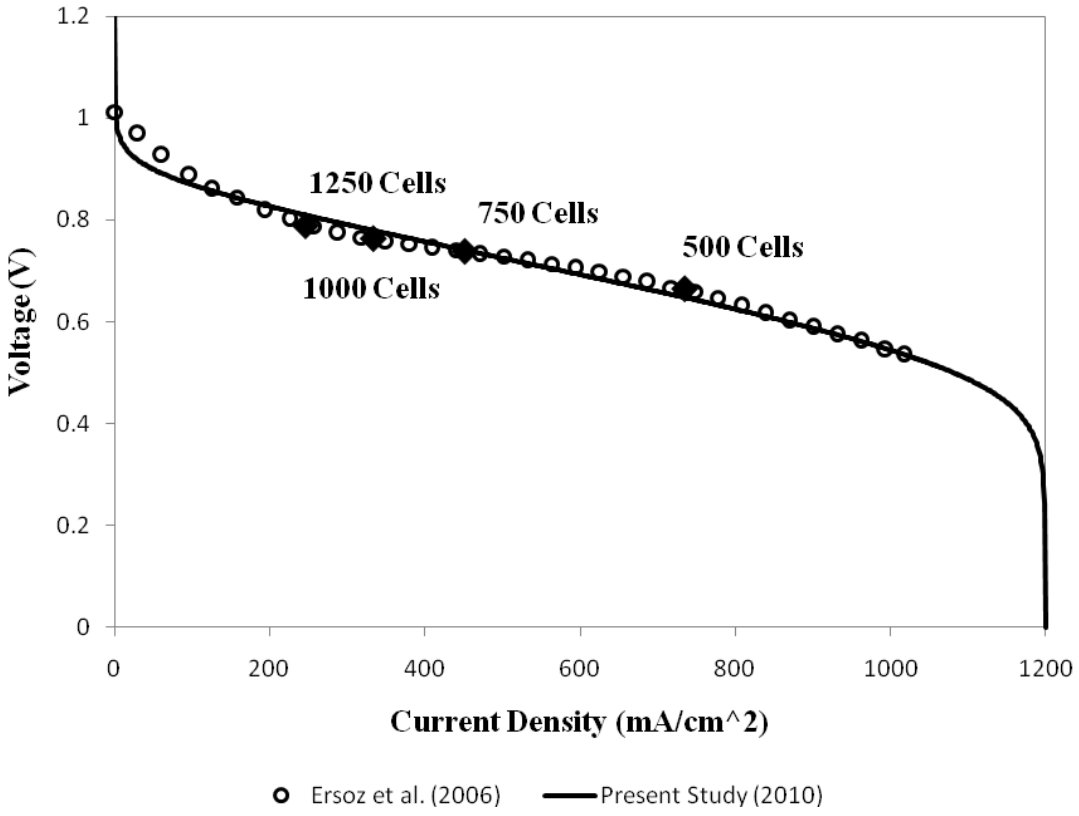

Figure 4.10. Polarization curve comparison with Ersoz et al. (2006), showing current/voltage output for given stack sizes

Table 4.2. Comparison of calculated efficiencies of various fuel cell stack sizes

Number of Cells	1250	1000	750	500
Ersoz et al.	64.6	62.6	60.5	54.2
Present Study	66.5	64.6	61.5	54.5
% Difference	2.9	3.2	1.7	0.48

Further comparisons were made to test the model's ability to account for a change in reactant pressure. Similar to the Ersoz et al. comparison, the model parameters were adjusted so that the model output fit fuel cell data presented by Kim et al. (1995) at 1 atm

pressure. The model pressure was then changed while all other inputs and parameters were held constant. The resulting output as compared to actual fuel cell data presented by Kim et al. can be seen in Figure 4.11. Clearly the model somewhat failed to accurately accommodate the change in pressure. The pressure change is only accounted for in the model by the Nernst Equation (Equation 6). This ignores the change in bulk reactant concentration and the effect that has on the mass transport losses in the cell (Equations 46, 50, and 51).

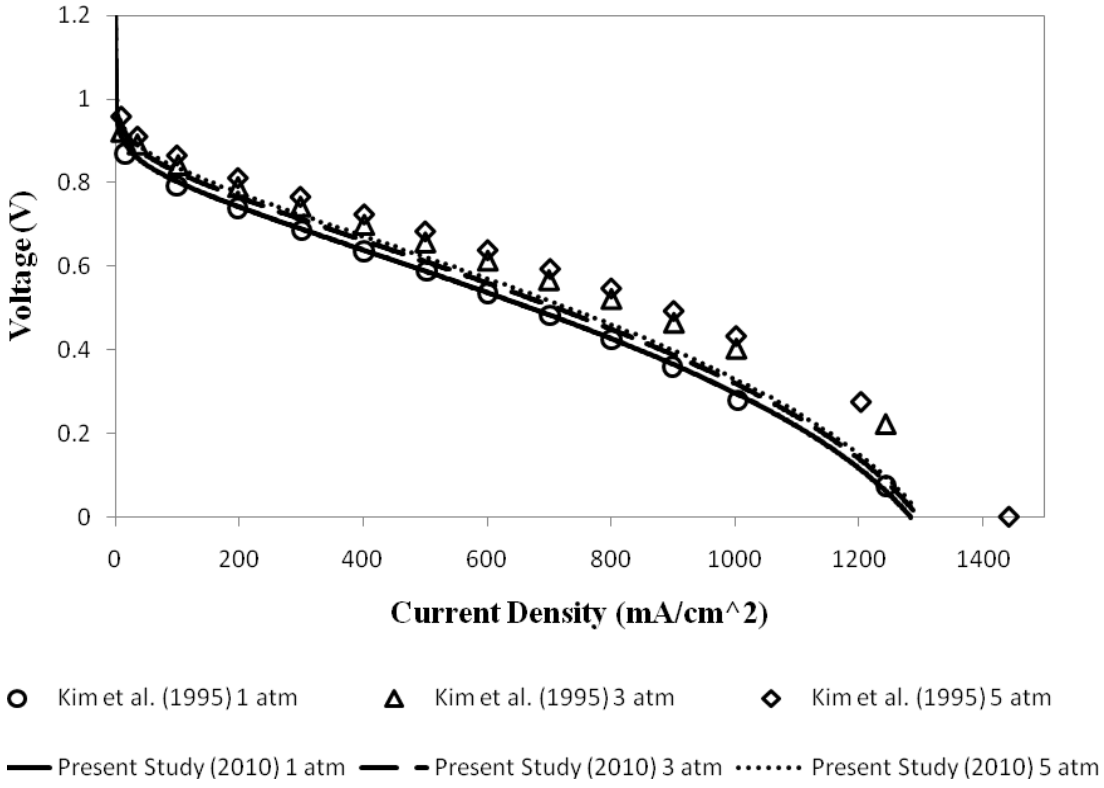

Figure 4.11. Comparison of polarization curves at various reactant pressures

Kim et al. also presented data for the same fuel cell at an increased temperature. The comparison between the fuel cell model and the experimental data can be seen in

Figure 4.12. The model shows a decreased voltage response at higher temperatures; this is due to the increase in activation losses as temperatures increase (Equation 7). The experimental data, however, shows a more complex interaction. From observation of Figure 4.12 in comparison with Figures 4.5, 4.6, and 4.7, it appears that the mass transport and ohmic overpotentials decrease with increasing temperature in a real fuel cell. It should be noted that the fuel cell model parameters can be set as temperature dependent arrays, but this was not considered since the main attraction of this model is its ease and speed of use, and creating arrays would require fitting multiple polarization curves over a range of temperatures.

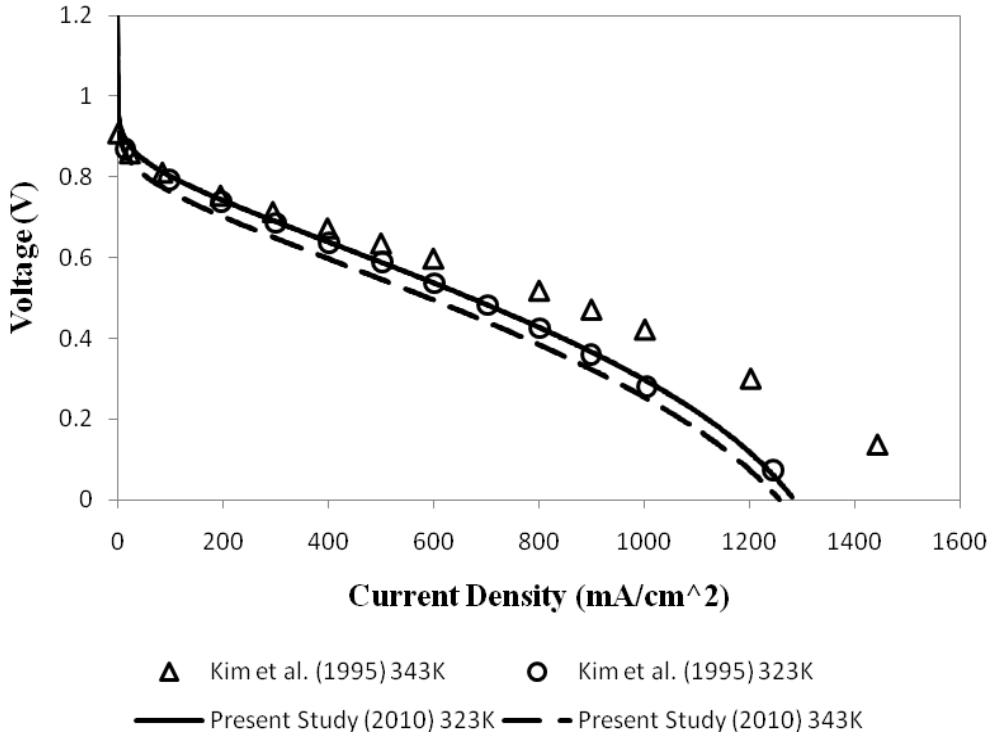

Figure 4.12. Comparison against fuel cell data at multiple temperatures at 1 atm

Kim et al. presented data on reduced oxygen concentrations and this can be used to corroborate the findings from Figure 4.12. Figure 4.13 shows that, as with the change in pressure, the model accounts for the change in Nernst voltage but does not take into account the increased mass transport losses that accompany a decrease in bulk reactant concentration.

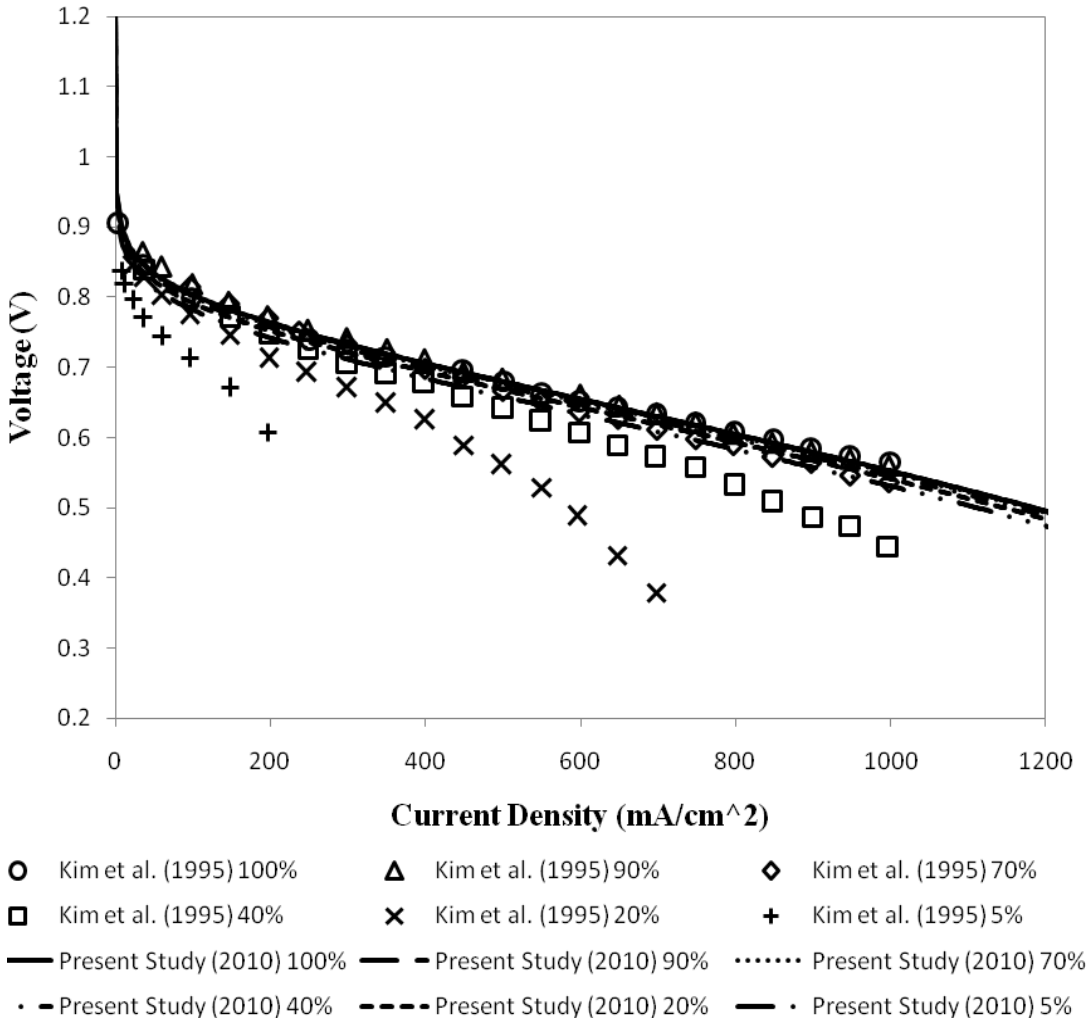

Figure 4.13. Fuel cell response at variable oxygen concentrations. Percent given is $\%O_2$ in the oxygen/argon cathode feed

4.4. VALIDATION OF HUMID PEM FUEL CELL MODEL

The PEM fuel cell model with the additional relationships detailed in section 3.4 shows substantial improvement over the standard model, though some of the results are still not ideal.

Figure 4.14 shows the same comparison as Figure 4.11, but with the new model. The model predictions are more accurate, especially at high current densities, though it appears that the model still under-predicts the decrease in mass transport losses at higher pressures. The inverse pressure relationship of D^{eff} in Equation 49 is a relationship that has been confirmed time and again, and if the ideal gas assumption made in Equation 51 is valid, this leaves the size of the diffusion layer as only possible source of the error. The majority of the diffusion layer is composed of the gas diffusion layer (GDL), typically a carbon cloth that forms an electrical connection between the catalyst and current collector, but the diffusion layer extends slightly beyond the GDL into the boundary layer of the gas stream. At increased pressures the viscosity of the gas stream increases, which in turn decreases the Reynolds number. At lower values of Reynolds number, the slope of the velocity in the boundary layer decreases which signifies a reduction in the percent of the flow channel at which diffusion is significant. This decrease in diffusion layer size and the corresponding decrease in mass transport losses is not accounted for in the model and could be responsible for the discrepancy in Figure 4.14.

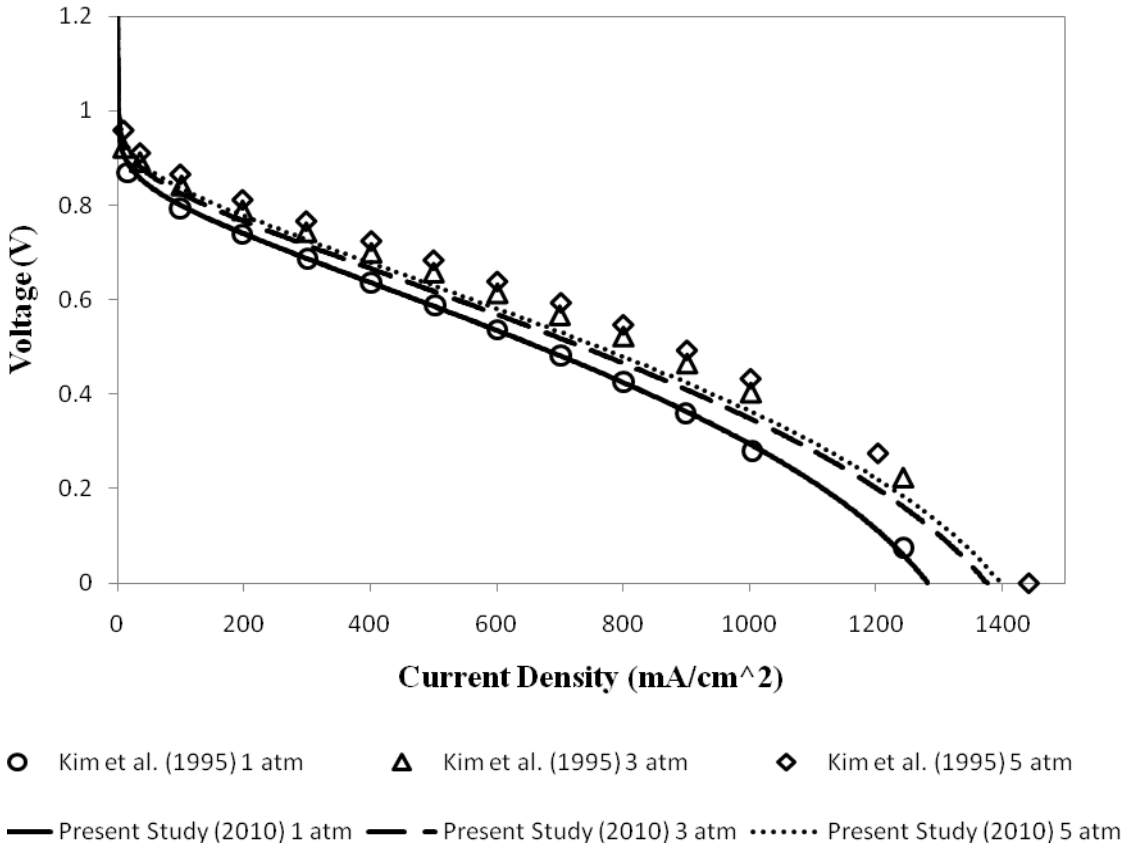

Figure 4.14. Comparison of humid model predictions with experimental data for the effects of pressure change

Figure 4.15 shows the same comparison as Figure 4.12, substituting the new model for the standard model. While the new comparison shows greater accuracy in the low current density region, mainly due to the increased exchange current density at elevated temperatures (Equation 54) offsetting the decrease in voltage observed in Figure 4.12, the results do not show great parity at medium to high current densities and there are two possible reasons for this.

The model may be under predicting the decrease in membrane resistance with respect to a temperature increase. The membrane used by Kim et al. was Nafion 115 which, while it is similar to the Nafion 117 membrane studied by Springer et al.

(resulting in Equations 41-44), has been shown by Yang et al. (2004) to follow a water uptake trend that differs from that of Nafion 117. This implies that that the resistance response of the membrane to changes in temperature is also different, but this question has not been addressed in the fuel cell literature.

Probably more significant is the disparity in apparent mass transport losses between the experimental and modeled data in Figure 4.15. The model predicts an overall reduction in limiting current density and hence an increase in mass transport losses; the reduction in bulk concentration due to increased temperature and water vapor pressure (required to maintain humidity levels at the increased temperature) in Equation 51 overwhelms the increase in effective diffusivity at increased temperatures implied by Equation 49. This is not seen in the experimental data, implying that there is a phenomenon at work that has not been taken into account by the model. Zhou et al. (2009) reported on membrane swelling increasing due to increased temperature and relative humidity, and suggested that, "GDL deformation reduces gas flow area and through-plane thickness, which can facilitate the gas flow [and] therefore reduce flow resistance." They also stated that membrane swelling reduces contact resistance between the GDL and current collector, reducing ohmic losses.

Error could also be attributable to a discrepancy between reported fuel cell temperature and average cell temperature. The fuel cell model presented here considers the average membrane temperature of the fuel cell, but Le et al. (2008) illustrated clearly that there exists a great variation in temperature across the membrane. It was assumed that the temperature reported was an average, but this may not be correct.

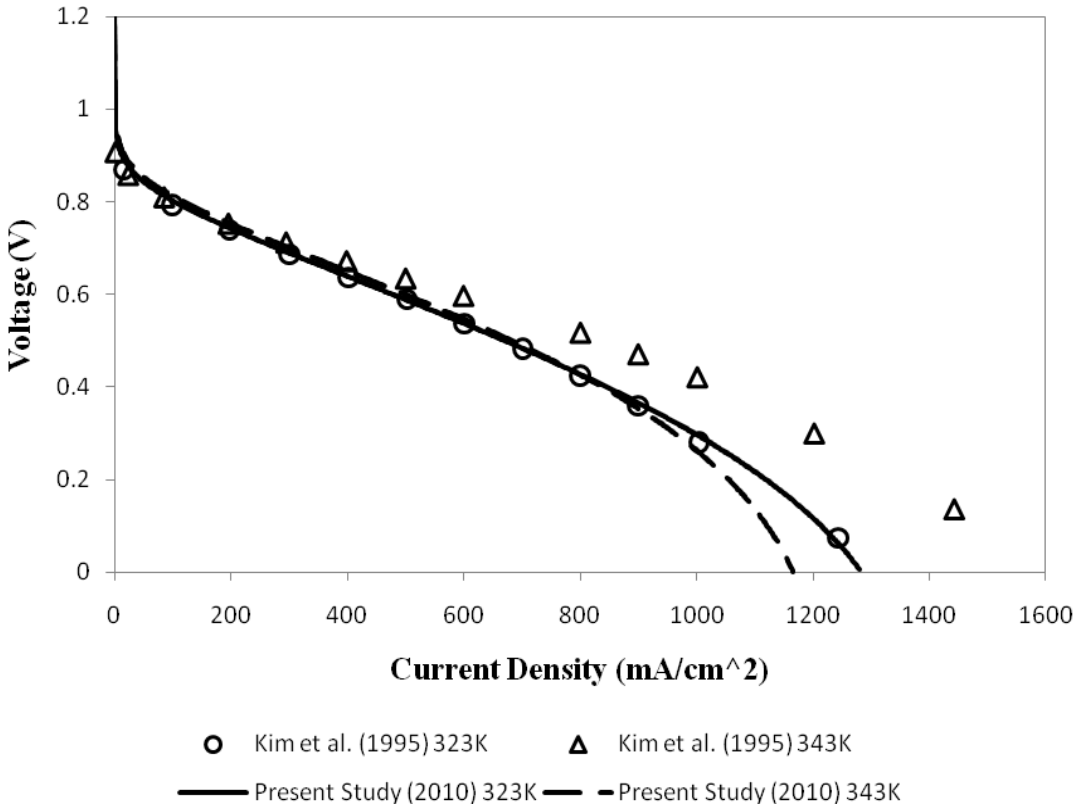

Figure 4.15. Comparison of humid model predictions with experimental data for the effects of temperature change

The new model predictions seen in Figure 4.16 are much improved from those of the standard model predictions from Figure 4.13. The model shows the same trend of increased mass transport losses at low reactant concentrations that the experimental data shows, however this increase in losses is over predicted by the model. The model does not take into account the change in diffusivity of oxygen as the percent of argon increases, but if this were taken into account it would result in lower oxygen diffusivities (Fuller et al., 1966) and consequently less accurate model predictions. Argon, being a noble gas, is most likely not causing a change in the GDL thickness, and the difference in viscosity between it and oxygen is unlikely to be responsible for so large a deviation between predicted and actual mass transport losses. If the ideal gas assumption in

Equation 51 is valid, then there is nothing in the theory laid out in Section 3.4.1.3 for predicting mass transport losses that should be suspected of error. Consequently, the source of the discrepancy between the experimental and predicted polarization curves in Figure 4.16 remains an open question.

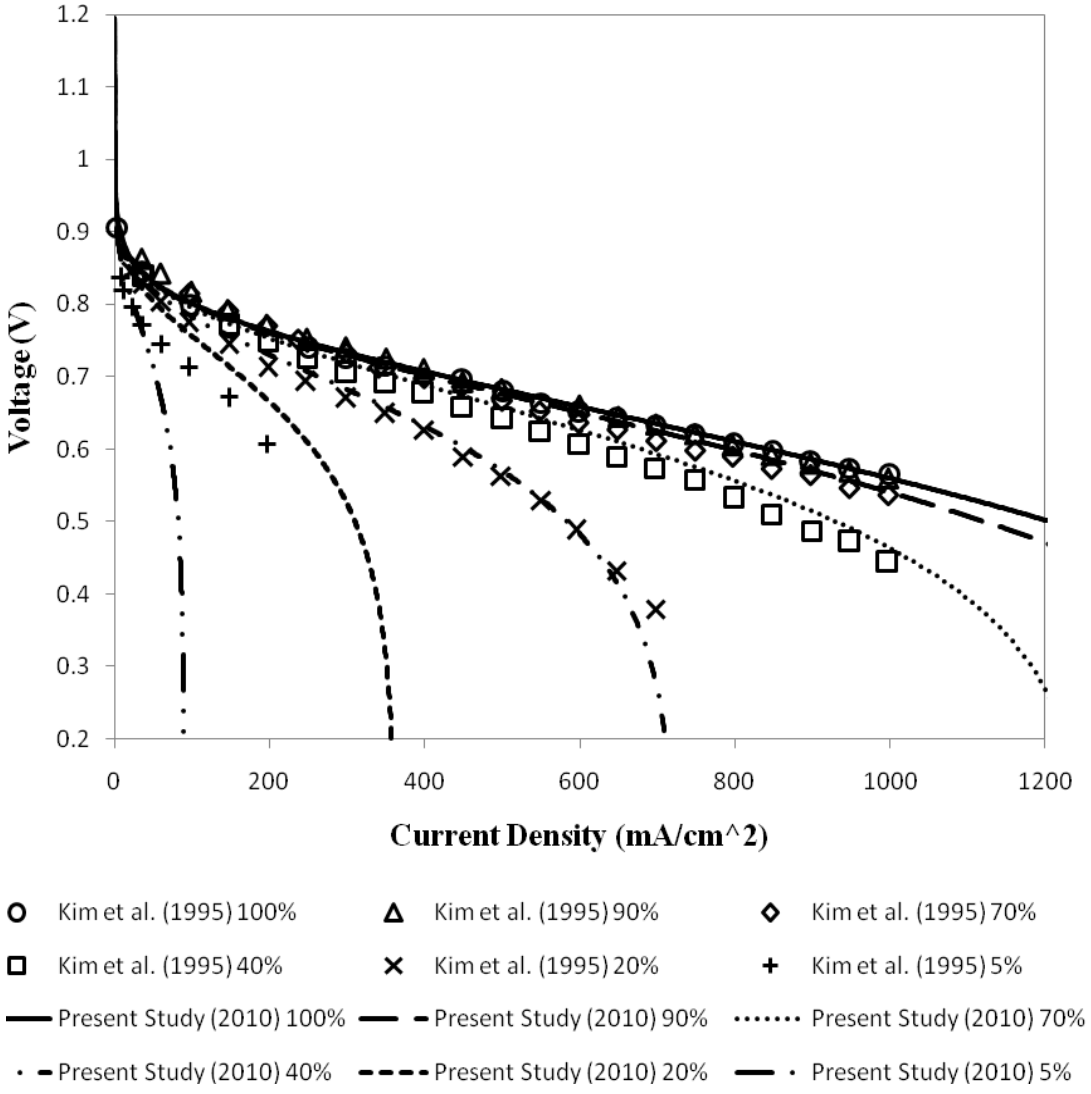

Figure 4.16. Comparison of humid model predictions with experimental data for the effects of changing oxygen concentration in an O_2/Ar mixture

Figure 4.17 compares model predictions for the effects of a change in the relative humidity of inflow gasses. Here the polarization curve was matched to data collected at 70% relative humidity by Yan et al. (2006). When the humidity is increased to 100%, the mass transport losses increase due to oxygen being displaced by water vapor in the cathode, but this is offset at lower current densities by the decreased membrane resistance that results from increased water content of the membrane. The increased diffusivity of oxygen through water vapor is not accounted for by the model, but this would increase the predicted limiting current density by less than 3%—not enough to account for the discrepancy between the modeled and experimental data. Another possible source of the disagreement between the two data sets lies with the membrane resistance and how polarization curves are generated experimentally. With a physical system, the current is increased from open circuit to short circuit. As the current increases, the amount of water produced by the cell increases in accordance with Equation 37. Liu and Wu (2006) showed that this reduced the membrane resistance as the test was run; instead of the straight line for ohmic overpotential shown in Figure 4.2, the slope would decrease as the current density increased. The modeling software, however, generates a polarization curve as a snapshot, using a single value for resistance. The result of this is that a polarization curve from a physical fuel cell would exhibit a higher voltage output than a model would as current density increased, but at high current densities this effect would be overwhelmed by the mass transport losses. This could partially explain the profile of the 100% relative humidity curve presented by Yan et al. (2006) and the discrepancy between it and the model prediction.

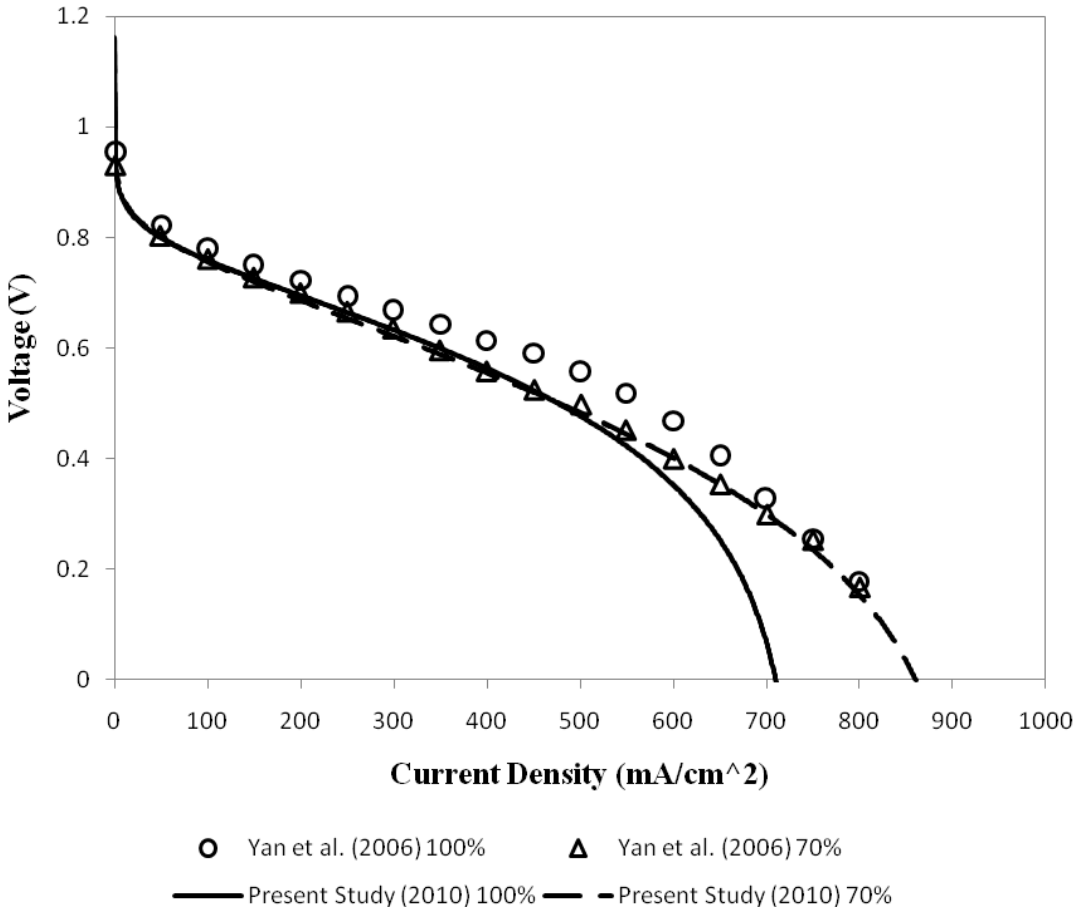

Figure 4.17. Comparison between predicted and reported performance after a change in relative humidity from 70% to 100%

Yan et al. (2006) also reported data that allowed the use of average relative humidity in Equation 34 to be tested. Figure 4.18 compares the model prediction for an average relative humidity of 85% with two data sets; one with the cathode stream humidified to 70% and the anode to 100%, and another with cathode at 100% and the anode at 70%. The average relative humidity of both of these data sets is 85%, and, if the average relative humidity assumption is accurate, the two should match, but, as can be seen, they are not equal and the model prediction falls between them.

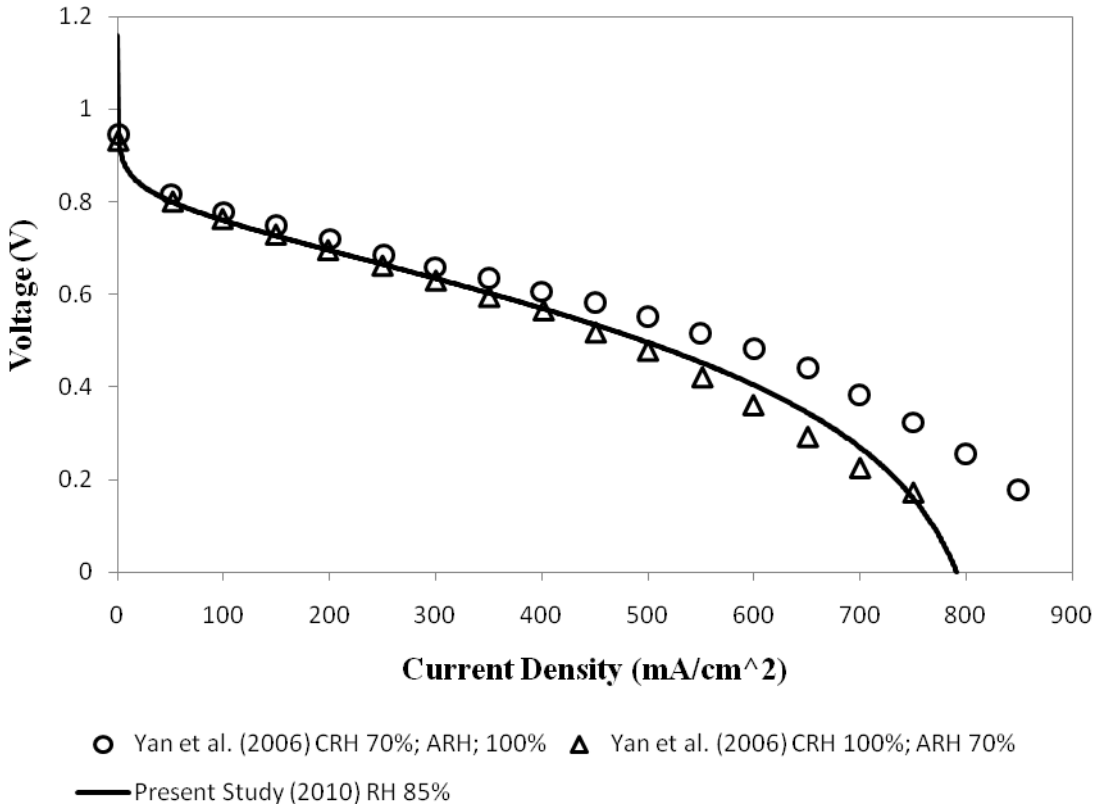

Figure 4.18. Comparison between non-symmetric humidification and the average humidity approximation

5. SUMMARY, CONCLUSIONS, AND RECOMMENDATIONS

The fuel cell model developed by Gamma Technologies was discussed and tested against independent data reported in the literature. It was found to be capable of reproducing the voltage/current response of actual fuel cells as well as the change in efficiency resulting from a change in current output from those cells. The model was shown to have insufficient predictive abilities when the conditions—temperature, pressure, and reactant mole fraction—from the copied polarization curve were changed. The model also had no mechanism to account for the effects of relative humidity. A model to relate the limiting current density to a change in bulk reactant concentration due to changes in water vapor content, temperature, pressure, and inlet oxygen mole fraction was therefore implemented. A model relating membrane water content, and hence membrane resistance to proton flow, to relative humidity was also included, as well as a relationship between exchange current density and temperature. These remedied many of the deficiencies of the standard model and allowed for it to respond more accurately to variable fuel cell operating conditions. The findings reported here established this model as capable of simulating PEM fuel cells with a reasonable degree of accuracy and the low computational intensity inherent to analytical modeling. Given the software environment the model is implemented in, this could be of significant aid to the design and optimization of fuel cell and hybrid powered vehicles.

This study highlights the need for more research in a number of areas. Most apparent is the need to develop empirical relationships for the formation of liquid water in the GDL at high water activity levels. Numerical solutions to two-phase flow have

been found, but an empirical analytic solution would allow for this important phenomenon to be incorporated into less computationally intensive models.

The cathode and anode in this study were considered as a single flow, but splitting them would allow the model more flexibility and accuracy. Yan et al. (2006) showed the divergence from stoichiometry of the fuel and oxidizer streams can have a large impact on cell performance. In considering the flows combined, this model and others (Sharifi Asl et al., 2010) also took an average relative humidity for calculation of membrane water content, but as has been shown in this study, this is not ideal. In order to separate the flows for an analytical model, relationships for electro-osmotic drag and water diffusion coefficients need to be found. Springer et al. (1991) did this for Nafion 117, though their diffusion coefficient relationship was stated to be only valid for $\lambda > 4$, and these relationships are likely invalid for other membranes used by PEM fuel cells.

The relationship between relative humidity and membrane resistance developed by Springer et al. has also not been extended to non-Nafion 117 membranes. This limits the model here, and many other fuel cell models as well, to a single choice of membrane type or reduced accuracy with other membranes. Furthermore, the Springer et al. resistance correlations are only valid for $\lambda > 1$, and this limits the ability for analytical models to predict fuel cell autohumidification, a topic of interest to designers of fuel cell vehicles. This should be remedied with detailed studies in the future.

APPENDIX A.

UNCERTAINTY ANALYSIS

Since this study has been largely qualitative in nature and devoid of experimental observations, formal uncertainty analysis is inapplicable. A form of analysis that considers the sensitivity of the model output to the input variables, however, could be used to give a sense of the benefit gained by improving a parameter of a fuel cell. By analyzing the voltage outputs given in Figures 4.3 through 4.7, at current densities of 400, 600, and 800 mA/cm^2, Table A.1 was developed. These current densities were chosen as representatives of useable range of fuel cell output.

Table A.1. Change in fuel cell output for given change in fuel cell parameter, at given current densities

Variable	from	to	% difference in variable	% difference in voltage output		
				400 mA/cm^2	600 mA/cm^2	800 mA/cm^2
R_i	0.005	0.0005	-90	14.9	25.7	40.3
	0.005	0.01	100	-16.5	-28.5	-81.0
i_l	1500	1000	933.3	8.0	12.4	18.3
	1500	2000	33.3	-7.3	-11.6	-17.3
i_o	0.001	0.0001	-90	-14.3	-16.5	-19.4
	0.001	0.01	900	14.3	16.5	19.4
C	75	50	-33.3	1.3	2.4	4.3
	75	100	33.3	-1.3	-2.4	-4.3
α	0.375	0.25	-33.3	-40	-47.6	-57.3
	0.375	0.5	33.3	20	23.8	28.7

These results could be used, if coupled with an economic analysis of the cost of fuel cell improvements, how to achieve the desired level of performance for the least possible expense. For example, it could hypothetically be determined that reducing the membrane thickness the most cost effective way to increase performance for their system (if the economic analysis determined that the reduced lifespan of a thinner membrane was less of a cost than increased platinum density, etc).

For the purpose of this study, it is sufficient to note that a large change in the variables given in Table A.1 is required to produce the modest change in output voltage. That is to say, for example, for the purposes of this software program, a fuel cell with a charge transfer coefficient of 0.4825 is qualitatively similar to one with a charge transfer coefficient of 0.83, and the difference can be neglected.

APPENDIX B.

HYDROGEN SAFETY CONSIDERATIONS

If hydrogen use is to become ubiquitous in our society, it is crucial to analyze safety standards already established and ensure that they are adequate. Many researchers (MacIntyre et al., 2007; Crowl and Jo, 2007; Dahoe and Molkov, 2006) and government organizations (Sandia National Laboratories, 2007) are doing just that. This section will seek to present in brief key considerations that need to be made in order to use hydrogen in a safe manner.

The hazards associated with hydrogen are similar to those for other fuels, and they differ where physical characteristics differ. Table A.2 compares some important properties of hydrogen with those of natural gas and gasoline. One of the most significant differences is hydrogen's very low density. This makes it very buoyant; hydrogen rises much more rapidly than other fuels when leaks occur. This is illustrated in Figure A.1, which shows a simulation of hydrogen (case b) after release compared with the more placid spread of methane (case c) and ethylene (case d) (Vudumu et al., 2009b).

Hydrogen's rapid rise coupled with its wide flammability limits is significant because it implies that even a small leak could lead to accumulation of a flammable hydrogen mixture in partially enclosed areas such as parking garages, road tunnels, or between rafters in a building (Gupta et al., 2007; Koylu et al, 2009). This implies that, were a fire to occur, it would be more likely to happen overhead (Koylu et al., 2009), as opposed to at ground level, as would be the case with more dense fuels. A hydrogen flame that begins at ground level will tend to rise rapidly. This is illustrated in the

Table A.2. Comparison of properties of hydrogen, natural gas, and gasoline

Characteristic	Hydrogen	Natural Gas	Gasoline
Lower heating value (kJ/g)	120	50	44.5
Flammability limits in air (vol%)	4-74	5-15	1-7
Density (kg/m^3)	0.082	0.67	4.4
Diffusion Coefficient in air (cm^2/s)	0.61	0.16	0.05
Stoichiometric flame speed (m/s)	2.1	0.4	0.3
Minimum ignition energy (mJ)	0.02	0.3	0.3

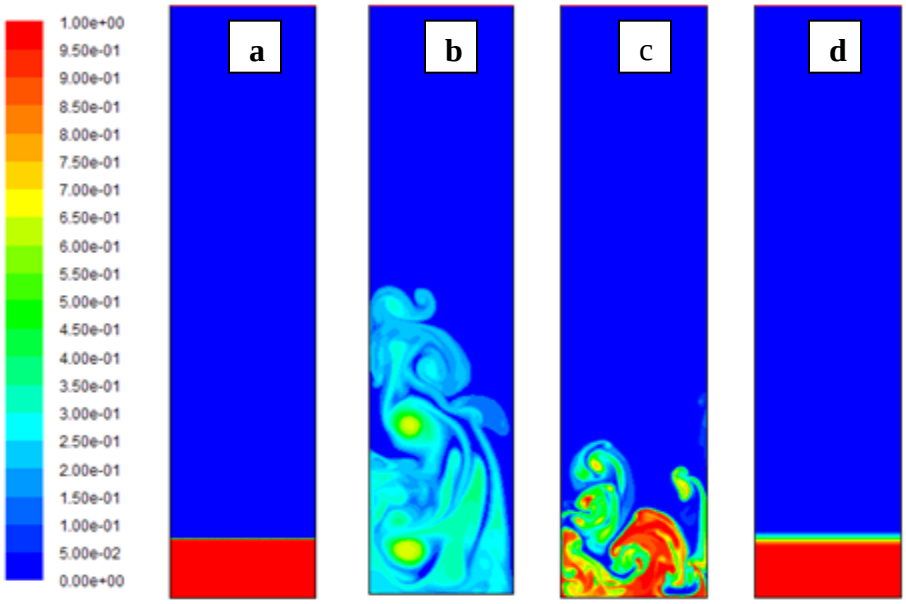

Figure A.1. The transient mixing behavior of gases a) initially concentrated in the lower 10% of the cylinder. b) Hydrogen/air, c) methane/air and d) ethylene/air mixing 2 seconds after the release of the fuel (Vudumu et al., 2009b). Scale is percent fuel in mixture by volume

tragedy of the Hindenburg disaster. Two thirds of the passengers on the Hindenburg survived, as the fire raged above their heads. Those that did die were either located at the front tip of the zeppelin (which, as the back sank, became an exit point for hydrogen), jumped, or became trapped as the wreckage settled around them, and died as a result of burning diesel fuel (Russell, 2009).

The accumulation of hydrogen is a cause for specific concern, since hydrogen (like other flammable gasses) has a tendency to detonate when ignited in confined areas. The wide flammability limits and low minimum ignition energy exacerbate this issue. There are three distinct aspects to the mitigation of this hazard: sensors for early detection, ventilation to prevent accumulation, and electrical grounding to avoid static discharges. Sensors are necessary because hydrogen is naturally an odorless gas. Odorants that are typically added to gasses (such as the methanethiol added to the natural gas used in homes) cannot be used with fuel cells, as they degrade the platinum catalyst. Sensors must be relied upon to warn of any leaks. The high buoyancy of hydrogen potentially makes ventilation simpler than it would be for other fuels. Barley (2007) showed that even non-mechanical ventilation (no fan or other energy input) is capable of reducing concentrations resulting from sizeable leaks to safe levels. An open vent in the right location could well be sufficient to evacuate hydrogen to the outside environment.

Hydrogen flames are different from flames of hydrocarbon fuels not just because of the properties of hydrogen, but also because of the properties of the combustion products. When hydrocarbons are combined with oxygen in combustion, soot is produced. As they are heated by the released chemical energy of combustion, they act as blackbody radiators. This radiation transfers heat to the surroundings and makes the

flame visible. Since hydrogen fires do not produce soot, they are much harder to see and are typically invisible under normal daylight conditions. Figure A.2 compares hydrogen and acetylene flames. The hydrogen flame is only visible because of the low light conditions, while the acetylene flame radiates with enough intensity to be seen at all times.

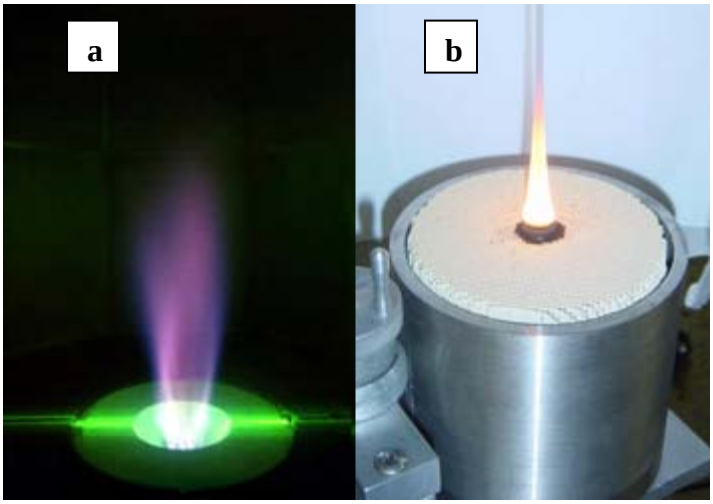

Figure A.2. Visibility comparison of a) hydrogen flame and b) acetylene flame

Besides just reducing visibility of the flame, the lack of radiating soot particles also diminishes the ability of a person to detect a hydrogen fire by sense of touch. A radiating fire can be felt at a distance, not just by convection, but by the absorption of the electromagnetic radiation put off by the hot soot particles. The practical consideration of this is that a hydrogen flame may not be felt on the skin until a person is nearly within the flame itself.

Hydrogen also affects all metals and most other materials it comes in contact with, resulting in a general weakening and embrittlement of the material. The National

Aeronautics and Space Administration's hydrogen safety standards (NSS 1740.16) give several recommendations to avoid embrittlement:

1. Aluminum is one of the few metals known to show only minimal susceptibility to hydrogen, so its use effectively eliminates hydrogen embrittlement.
2. Containers with thick walls of low-strength metals will generally contain hydrogen more safely than containers fabricated from similar alloys treated for high strength, subject to appropriate welding techniques.
3. A metal or alloy is almost certain to have a lower resistance to fatigue than if hydrogen were not present if it is exposed to hydrogen and cyclic stresses. Designers should, in the absence of data, assume a substantial (up to fivefold) decrease in resistance to fatigue.
4. The use of metals and alloys with a body centered cubic crystal structure, such as iron and tungsten, should be avoided whenever practical. Cast iron shall not be used.
5. Hydride-forming metals and alloys should not be used as structural materials for hydrogen service. Their use requires careful consideration of operating temperatures and adverse effects of hydride formation.

Several organizations have developed codes and standards for the safe handling and use of hydrogen and hydrogen fuel cells, including the National Fire Protection Association (NFPA), the International Electrotechnical Commission (IEC), the American National Standards Institute (ANSI), Underwriters Laboratories Inc. (UL), the Compressed Gas Association (CGA), the Society of Automotive Engineers (SAE), and the International Code Council (ICC). Standards are available covering a wide range of

possible safety issues. A sample of standards that can be consulted for detailed information is presented in Table A.3.

Table A.3. Relevant codes and standards

Code or Standard	Topic
NFPA 853	Standard for the Installation of Stationary Fuel Cell Power Systems
NFPA 50A	Gaseous hydrogen systems at consumer sites
IEC 62282-2	Fuel cell technologies - Part 2: Fuel cell modules
ICC IFC-2006	International fire code
ANSI/CSA America FC 1-2004	Stationary Fuel Cell Power Systems
UL 2075-2007	Gas and Vapor Detectors and Sensors
CGA P-12	Safe Handling of Cryogenic Liquids
CGA G-5.5	Hydrogen Vent Systems
SAE J 2578 (SAE J2578)	Recommended Practice for General Fuel Cell Vehicle Safety
NFPA 55-2003	Standards for the Storage, Use and Handling of Compressed Gases and Cryogenic Fluids in Portable and Stationary Containers, Cylinders, and Tanks, 2005 Edition

BIBLIOGRAPHY

Barley, C.D. and Gawlik, K. (2009). Analysis of buoyancy driven ventilation of hydrogen from buildings. *International Journal of Hydrogen Energy*, 34: 5592-5603.

Bernardi, D.M. and Verbrugge, M.W. (1992). A mathematical model of the solid-polymer-electrolyte fuel cell. *Journal of the Electrochemical Society*, 138: 2477-2491.

Berning, T., Lu, D.M., and Djilali, N. (2002). Three-dimensional computational analysis of transport phenomena in a PEM fuel cell. *Journal of Power Sources*, 106: 284-294.

Biyikoglu, A. (2005). Review of proton exchange membrane fuel cell models. *International Journal of Hydrogen Energy*, 30: 1181-1212.

Buchi, F.N. and Srinivasan, S. (1997). Operating proton exchange membrane fuel cells without external humidification of the reactant gases. *Journal of the Electrochemical Society*, 144: 2767-2772.

Crowl, D.A., and Jo, Y. (2007). The hazards and risks of hydrogen. *Journal of Loss Prevention in the Process Industries*, 20(2): 158-164.

Dahoe, A.E., and Molkov, V.V. (2006). On the development of an international curriculum on hydrogen safety engineering and its implementation into educational programmes. *International Journal of Hydrogen Energy*, 32: 1113-1120.

Dawes, L.E., Haspal, N.S., Family, N.S., and Turan, A. (2009). Three-dimensional CFD modeling of PEM fuel cells: an investigation into the effects of water flooding. *Chemical Engineering Science*, 64: 2781-2794.

Dutta, S., Shimpalee, S., and Van Zee, L.W. (2000). Three-dimensional numerical simulation of straight channel PEM fuel cells. *Journal of Applied Electrochemistry*, 30: 135-146.

Ersoz, A., Olgun, H., and Ozdogan, S. (2006). Simulation study of a proton exchange membrane (PEM) fuel cell system with autothermal reforming. *Energy*, 31: 1490-1500.

Fontes, G., Turpin, C., Astier, S., and Meynard, T.A. (2007). Interactions between fuel cells and power converters: influence of current harmonics on a fuel cell stack. *IEEE Transactions on Power Electronics*, 22: 670-678.

Fuller, E.N., Schettler, P.D., and Giddings, J.C. (1966). A new method for prediction of binary gas-phase diffusion coefficients. *Industrial and Engineering Chemistry*, 58: 18-27.

Fuller, T.F. and Newman, J. (1993). Water and thermal management in solid-polymer electrolyte fuel cells. *Journal of the Electrochemical Society*, 140: 1218-1225.

Goswami, D., Mirabal, S., Goel, N., and Ingley, A. (2003). A review of hydrogen production technologies. *Fuel Cell Science, Engineering and Technology: First International Conference on Fuel Cell Science, Engineering and Technology, USA*, 61-74.

Gupta, S., Brinster, J., Studer, E., and Tkatschenko, I. (2009). Hydrogen related risks within a private garage: Concentration measurements in a realistic full scale experimental facility. *International Journal of Hydrogen Energy*, 34: 5902-5911.

Kim, J., Lee, S.M., and Srinivasan, S. (1995). Modeling of proton exchange membrane fuel cell performance with an empirical equation. *Journal of the Electrochemical Society*, 142: 2670-2674.

Koylu, U.O., Vudumu, S.K. and Sheffield, J.W. (2009). Hydrogen Safety in Accidental Release Scenarios. *Missouri Energy Summit, Columbia, MO*, April 2009.

Le, A.D., Zhou, B. (2008). A general model of proton exchange membrane fuel cell. *Journal of Power Sources*, 182: 197-222.

Liu, Q. and Wu, J. (2006). Multi-resolution PEM fuel cell model validation and accuracy analysis. *Journal of Fuel Cell Science and Technology*, 3: 51-61.

MacIntyre, I., Tchouvelev, A.V., Hay, D.R., Wong, J., Grant, J., and Benard, P. (2007). Canadian hydrogen safety program. *International Journal of Hydrogen Energy*, 32: 2134-2143.

Maggio, G., Recupero, V., and Pino, L. (2001). Modeling polymer electrolyte fuel cells: an innovative approach. *Journal of Power Sources*, 101: 275-286.

Mazumder, S. and Cole, J.V. (2003). Rigorous 3-D mathematical modeling of PEM fuel cells. *Journal of the Electrochemical Society*, 150: A1503-A1509.

Meng, H. and Wang, C.Y. (2004a). Electron transport in PEMFCs. *Journal of the Electrochemical Society*, 151: A358-A367.

Meng, H. and Wang, C.Y. (2004b). Large-scale simulation of polymer electrolyte fuel cells by parallel computing. *Chemical Engineering Science*, 59: 3331-3343.

Murgia, G., Pisani, L., Valentini, M., and D'Aguanno, B. (2002). Electrochemistry and mass transport in polymer electrolyte membrane fuel cells. *Journal of the Electrochemical Society*, 149: A31-A38.

National Aeronautics and Space Administration: Office of Safety and Mission Assurance. Safety Standard for Hydrogen and Hydrogen Systems. NSS 1740.16.

Nguyen, T.V. and White, R.E. (1993). A water and heat management model for proton-exchange-membrane fuel cells. *Journal of the Electrochemical Society*, 140: 2178-2186.

O'Hayre, R., Fabian, T., Lister, S., Prinz, F.B., and Santiago, J.G. (2007). Engineering model of a passive planar air breathing fuel cell cathode. *Journal of Power Sources*, 167: 118-129.

Pisani, L., Murgia, G., Valentini, M., and D'Aguanno, B. (2002a). A working model of polymer electrolyte fuel cells. *Journal of the Electrochemical Society*, 149: A898-A904.

Pisani, L., Murgia, G., Valentini, M., and D'Aguanno, B. (2002b). A new semi-empirical approach to performance curves of polymer electrolyte fuel cells. *Journal of Power Sources*, 108: 192-203.

Rajani, B.P.M. and Kolar, A.K. (2007). A model for a vertical planar air breathing PEM fuel cell. *Journal of Power Sources*, 164: 210-221.

Russell, P. (2009, October 25). Passengers aboard LZ 129 Hindenburg – May 3-6, 1937. Message posted to http://facesofthehindenburg.blogspot.com/2009/10/passengers-aboard-lz-129-hindenburg-may.html

Sandia National Laboratories 2007. *Hydrogen safety, codes, and standards.* Retrieved from http://www.ca.sandia.gov/8700/projects/content.php?cid=183

Sharifi Asl, S.M., Rowshanzamir, S., and Eikani, M.H. (2010). Modelling and simulation of the steady-state and dynamic behavior of a PEM fuel cell. *Energy*, 35: 1663-1646.

Springer, T.E., Zawodzinski, T.A., and Gottesfeld, S. (1991). Polymer electrolyte fuel cell model. *Journal of the Electrochemical Society*, 138: 2334-2342.

Vudumu, S.K., and Koylu, U.O. (2009a). A computational study on performance, combustion and emission characteristics of a hydrogen-fueled internal combustion engine. *Proceedings of ASME IMECE2009* -11183.

Vudumu S.K., and Koylu, U.O. (2009b). Detailed simulations of the transient hydrogen mixing, leakage and flammability in air in simple geometries. *International Journal of Hydrogen Energy*, 34: 2824-2833.

Wahiduzzaman, S., Kolade, B., and Buyuktur, S. (2004). An integrated proton exchange membrane fuel cell vehicle model. *SAE Technical Paper Series*, 2004-01-1474.

Wang, Z.H., Wang, C.Y., and Chen, K.S. (2001). Two-phase flow and transport in the air cathode of proton exchange membrane fuel cells. *Journal of Power Sources*, 94: 40-50.

Yamada, H., Hatanaka, T., Murata, H., and Morimoto, Y. (2006). Measurement of flooding in gas diffusion layers of polymer electrolyte fuel cells with conventional flow field. *Journal of the Electrochemical Society*, 153: A1748-A1754.

Yan, Q., Toghiani, H., and Causey, H. (2006). Steady state and dynamic performance of proton exchange membrane fuel cells (PEMFCs) under various operating conditions and load changes. *Journal of Power Sources*, 161: 492-502.

Yang, C., Srinivasan, S., Bocarsly, A.B., Tulyani, S., and Benziger, J.B. (2004). A comparison of physical properties and fuel cell performance of Nafion and zirconium phosphate/Nafion composite membranes. *Journal of Membrane Science*, 237: 145-161.

Zawodzinski, T.A., Neeman, M. Sillerud, L.O., and Gottesfeld, S. (1991). Determination of water diffusion coefficients in perfluorosulfonate ionomeric membranes. *Journal of Physical Chemistry*, 95: 6040-6044.

Zeman, J. Personal correspondence, Febuary 17, 2010.

Zhou, Y., Lin, G., Shih, A.J., and Hu, S.J. (2009). Assembly pressure and membrane swelling in PEM fuel cells. *Journal of Power Sources*, 192: 544-551.

VITA

Steven Francis Rodgers was born in 1985. He earned his Bachelor's degree in Mechanical Engineering from the University of Missouri–Rolla in May 2008. Requirements for a M.S. in Mechanical Engineering from the Missouri University of Science and Technology were completed in July 2010, and the diploma for that degree was awarded in August 2010.